AN IMPROVED METHOD FOR MEASUREMENT OF RADIAL THERMAL CONDUCTIVITY OF CYLINDRICAL BODIES

by

SALWA SHAIK

Presented to the Faculty of the Graduate School of

The University of Texas at Arlington in Partial Fulfillment

of the Requirements

for the Degree of

MASTER OF SCIENCE IN MECHANICAL ENGINEERING.

THE UNIVERSITY OF TEXAS AT ARLINGTON

May 2017

Acknowledgements

I would like to sincerely thank my advisor, Dr. Ankur Jain, for encouraging me and instilling confidence in me. I will be forever be grateful to him for permitting me to be a part of a the wonderful Micro scale thermo-physics laboratory. It is commendable how he patiently nurtured me and provided guidance throughout.

I would like to thank my fellow lab mates who were readily available to help troubleshoot when needed and who inspired me largely. I would also like to thank my parents for supporting me through school.

May 21, 2017

Abstract

AN IMPROVED METHOD FOR MEASUREMENT OF RADIAL THERMAL CONDUCTIVITY OF CYLINDRICAL BODIES

by

Salwa Shaik, MS

The University of Texas at Arlington, 2017

Li-ion cells are ubiquitously found in day to day electronic devices due to their high power density storage capacity. These batteries are known to exhibit sharp reduction in performance at high temperature. Due to this, several attempts have been made in the past to measure thermal properties of the Li-ion cell. This work improves upon past measurements by showing that heat loss during measurements is non-negligible, and by developing an analytical model to account for such heat loss. Experimental measurements carried out on multiple materials demonstrate non-negligible heat loss. When accounted analytically, these data result in thermal conductivity values that are in close agreement with independently-measured values for Acrylic and Delrin. A D-optimality criterion is used for improving measurement accuracy. Measurements are also carried out on a Li-ion cell in order to accurately determine its radial thermal conductivity. The accurate measurement of thermal properties enabled by this work may facilitate improved thermal design of Li-ion based energy conversion and storage devices.

Supervising Professor: Ankur Jain

Table of Contents

List of Illustrations

List of Tables

Chapter 1

Motivation for research

Li ion batteries are found today in most day-to-day electronic equipment. The Li ion are the most popular rechargeable batteries for mobile/portable electronics today, which offer high power density storage. These are widely used for electric automobiles, military equipment and aero planes. For the same size of two different batteries, a Li ion is known to hold large power density than any other electrochemical battery. Due to these advantages the Li ion have become a common replacement for Lead acid batteries.

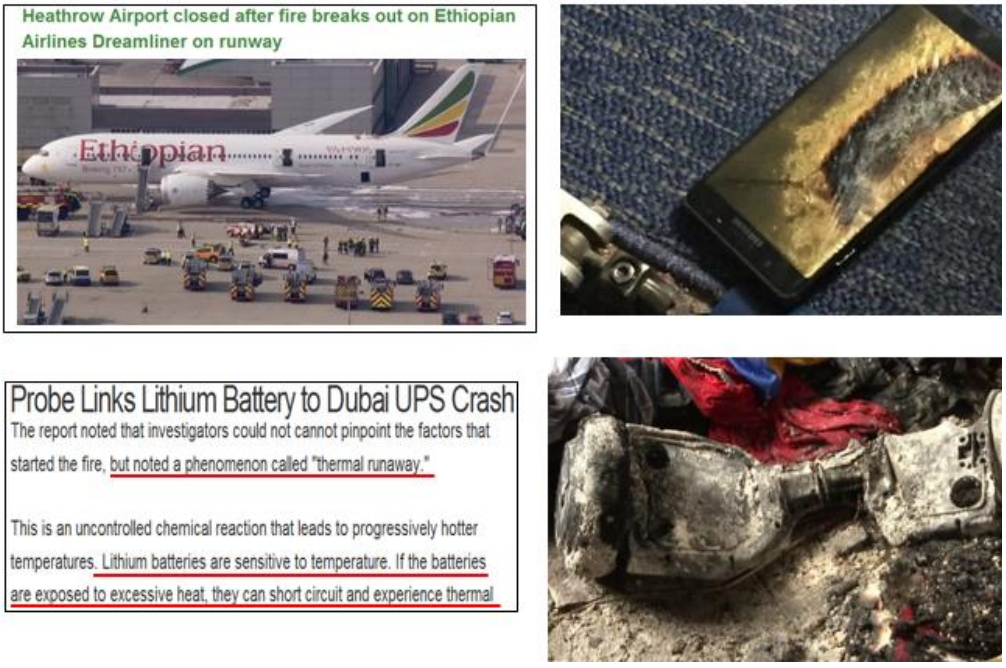

Figure 1 Images showing fatal accidents caused by thermal run away in Li ion cells [i] [ii] [iii] [iv]

NTSB traces Boeing 787 Dreamliner fire to battery cell, but questions remain

February 07, 2013 | By W.J. Hennigan

Email Share +1 1 Tweet 0

A month into investigating a fire that broke out on Boeing Co.'s grounded 787 Dreamliner passenger jets, the National Transportation Safety Board said it found a short-circuit in one of the aircraft's lithium ion batteries and even traced it to a specific cell, but still doesn't have a cause.

Speaking to reporters Thursday from Washington, NTSB Chairwoman Deborah Hersman said the agency hasn't reached a conclusion on the cause of the fire that occurred in Boston on Jan. 7. But investigators have been "working around the clock to learn about what happened and why."

Figure 1 Images showing fatal accidents caused by thermal run away in Li ion cells [v]

The battery however poses danger when operated at high temperature. The explosive nature of the Li-ion battery has proven to be lethal in many different instances. Several plug-in electric vehicle fire incidents have taken place since the introduction of mass-production plug-in electric vehicles in 2010. The U.S. National Highway Traffic Safety Administration (NHTSA) is conducting a study due in 2014 to establish whether lithium-ion batteries in plug-electric vehicles pose a potential fire hazard. In 2013 the NTSB traced a plane fire to a short circuited Li-ion cell, on investigation a term 'Thermal runaway' came into existence. The UPS plane crash in Dubai was also caused due to firing of a Li ion battery. The hover board mishaps, Samsung Note 7 blasts and many more are all pertained to Li-ion batteries. Figure 1 shows the images of some such fatal incidents.

The history of Li ion urges researchers to deliver conclusive results to prevent mishaps and develop quality engineering. Detailed understanding of the thermal properties of Li ion cells is the need of the time.

Chapter 2

Physics of Li-ion cells

A lithium-ion battery is an energy storage device providing electrical energy by chemical reactions that are exothermic in nature. The cylindrical cells have high energy density, high power, as well as high performance and longevity. The application of these batteries is multifold, for example, electric vehicles, laptops, portable electronic devices and power tools. These cylinders may also be packaged into units composed of multiple such cells; for example the Tesla roadster is made of 6,831 cylindrical lithium-ion cells (Eberhard).

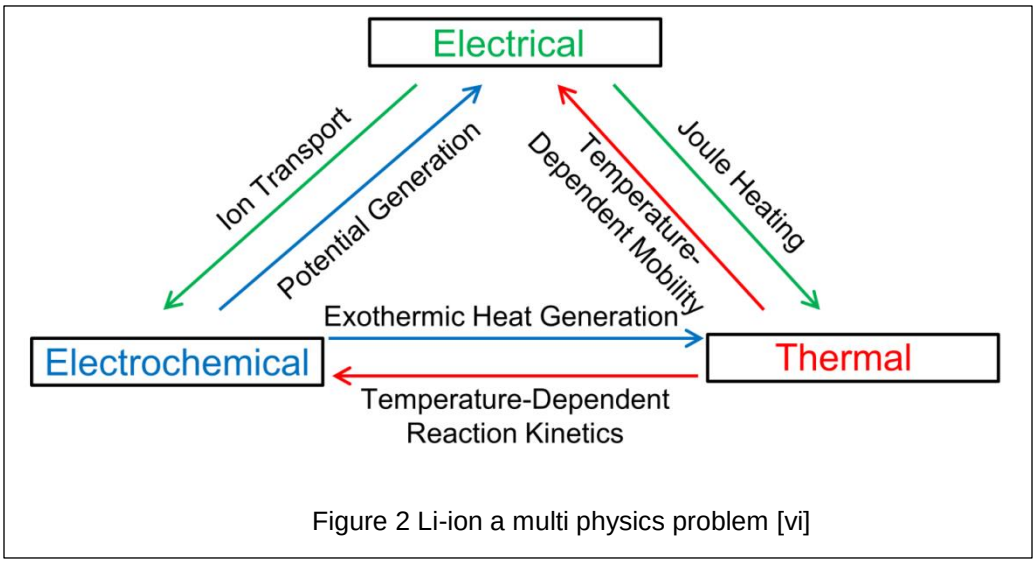

Figure 2 Li-ion a multi physics problem [vi]

The Li-ion cell is a Multi scale physics problem. There are multiple aspects of the cell that affect its functioning. This is shown in Figure 2. Electrochemistry, like in most battery cells plays a key role. Diffusivity of ions at a micro scale coexists along with heat transfer and stress generation within a Li-ion cell. The relation between chemical reaction

and heat determined by Arrhenius is well known. This makes it a dynamic coupled problem. However, for the scope of this thesis only the thermal aspect of the Li-ion cell is studied.

The cylindrical cell is made of an anode, a cathode, current collectors and a separator, all rolled into a bundle and immersed into electrolyte. Electrode tab protrusions are positioned at the end caps of the cell to conduct current to the outer cell terminals.

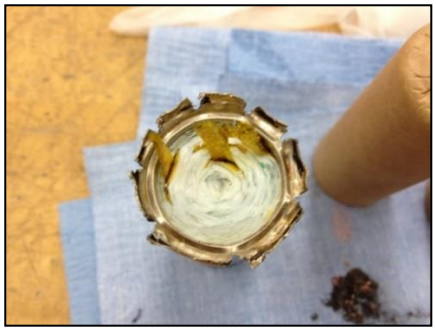

Figure 3(a): Spiral assembly of Li-ion cell [vii]

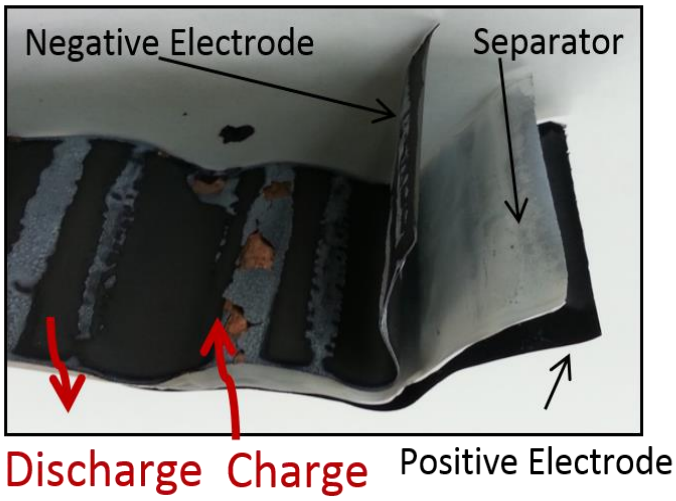

Figure 3(b): Layers in a Li-ion cell

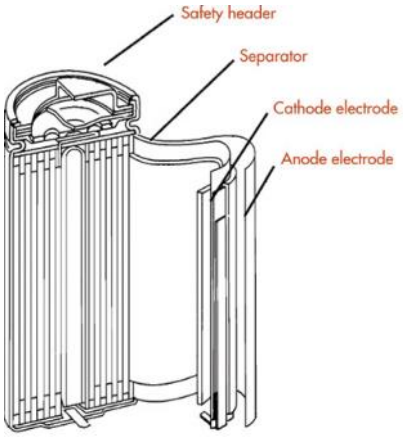

Figure 3(c): Li-ion anatomy [viii]

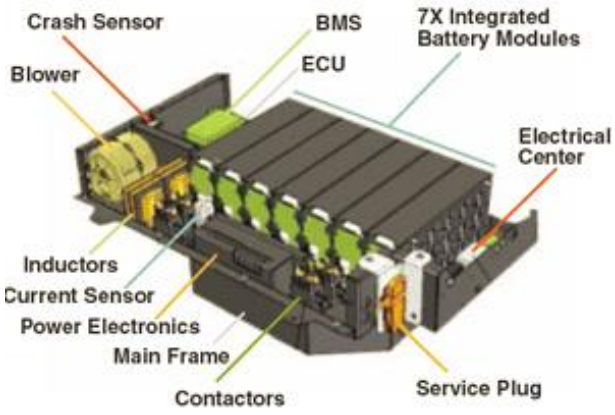

Figure 3(d): A cell pack [viii]

As shown in Figure 3(a). The layers are shown in figure 3(b). 3(c) depicts the anatomy of the cell construction, the safety vent, end caps etc. are all clearly shown. The Li ion may be used as a pack of multiple cells as shown in Figure 3(d).

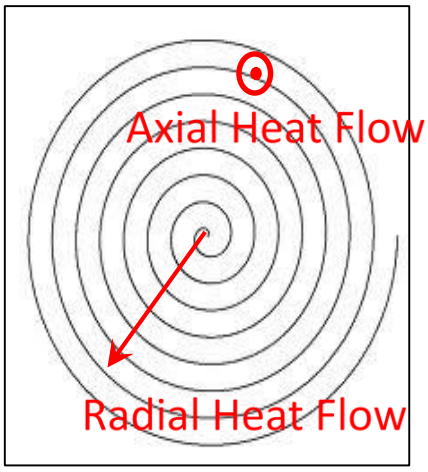

Figure 4 Anisotropy in thermal conductance in Li-ion cell

The major drawback of the Li ion batteries is that they are notoriously known to be volatile in nature at high temperature operation ranges. To prevent any mishaps optimal cooling of a Li ion battery is essential. To design appropriate cooling measures, the governing thermal properties of any entity i.e, the thermal conductivity (k W/m K) and heat capacity (C_p, J/kg K) are to be known. Heat capacity maybe easily determined by a simple calorimetry experiment. It is a challenging task to determine thermal conductivity of a cylindrically shaped cell. Sophisticated machines like the LFA or the hot disk plate TPS (Transient planar source) are available to determine thermal conductivities but these are specifically built for Cartesian and plane surface objects only. A methodology for cylindrical body is necessary to determine the thermal conductivity of over a Li ion cell.

Due to this construction, a strong anisotropy in thermal conductance is expected in the radial direction, unlike the axial direction. Attempting to determine thermal properties assuming isotropy may result in under prediction or over prediction of the properties. Heat flow in the radial direction is hindered by multiple contact resistances while in the axial direction the heat is channeled through the least obstructive path which is provided by the current collectors. A schematic of the radial and axial thermal conductance path is shown in Figure 4. Literature suggests that the radial thermal conductivity is two orders lesser than axial thermal conductivity in a Li ion cell. The radial thermal conductivity poses as the limiting factor in cooling of the cell. Hence, as the heat is accumulated in the radial direction, by accurately determining the radial thermal conductivity one can attempt to build appropriate cooling device to avoid fatalities.

Several papers have reported computational and experimental studies on temperature distribution at cell level and at pack level [3][4][5][6][7][8]. Calorimetry experiments to determine the heat capacity of some batteries have been reported in the past [9]. However, this calorimetry method does not provide the thermal conductivity of battery cells. A few papers report measurement of both thermal conductivity and heat capacity using steady state measurements through Xenon Flash Technology [10]. This is a costly and complicated approach which is not readily available.

One such paper that has suggested an affordable and relatively quick methodology to determine both heat capacity and thermal conductivity through one single experiment; is listed [1].

Chapter 3

Some sophisticated devices

Before we move ahead, here are some devices that can measure the thermal conductivity of different materials available in the market today. The thermal properties of Delrin, Acrylic materials are determined using the TPS (Transient planar source) device by hot disk, this is one of the few equipment available in the market to determine thermal conductivity. These measurements are later used to tally with the suggested model technique. The TPS is discussed here along with a few other devices.

A TPS instrument stand is displayed down below in 5(a). A suitable platform is

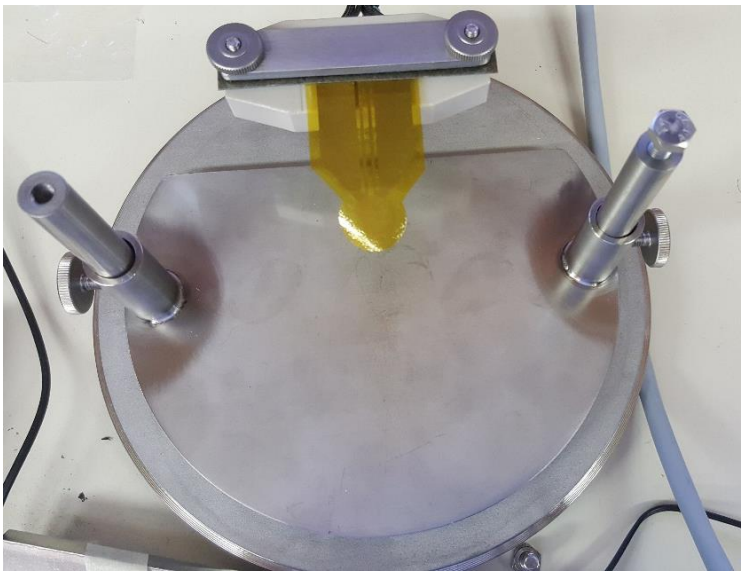

Figure 5 (a) Heater-sensor platform set up- A top view provided

where the sample is then positioned. The sensor is also the heating source. The sensor is a fragile filament that is connected to four conducting terminals. Power is supplied to the sensor through these four terminals. Once the sensor is securely placed onto the terminals

it is fixed in place using a simple screw-washer-plate mechanism. Then the sample is placed such that the sensor aligns to the sample's flat surface nicely. A weight is then placed onto the set up to minimize resistive air molecules at the sensor and sample contact surface. In case of a two sample method, two samples of the same material whose thermal conductivity is to be determined are mounted and the sensor is sandwiched between the two samples planar ends. This is shown in Figure 5(b).

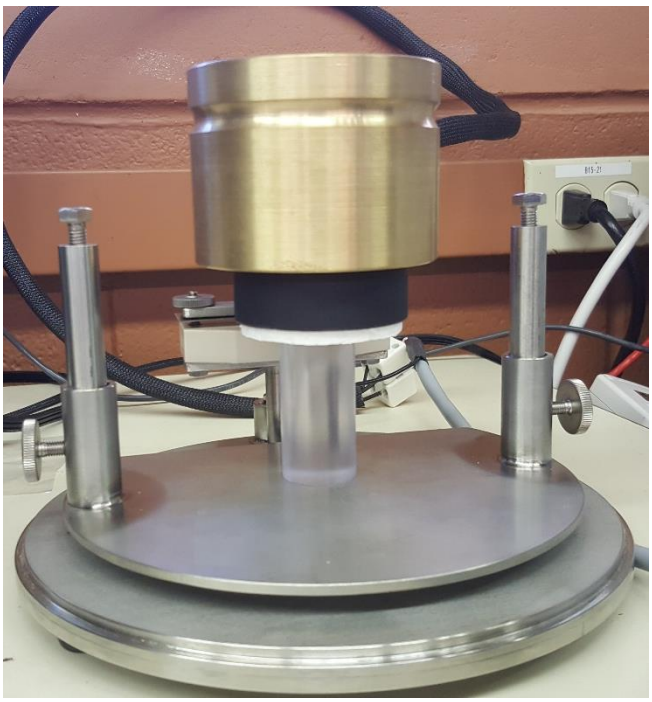

Figure 5(b) Single sided sample set up

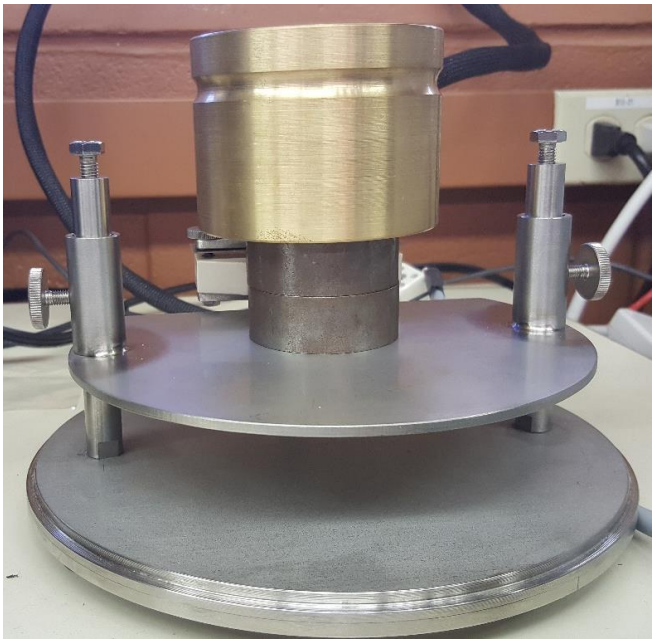

Figure 5(c) Double sided sample set up

The TPS instrument uses a simple *y=mx* format equation (1). Where P_0 is the power providing heat in Watt. This is input into the system by the user the effective radius a = [radius of sample-radius of sensor] is also user specified. $D(\tau)$ is computed by the equipment using some Fourier expansions given by $D(\tau)=\frac{1}{m^2(m+1)^2}\int_0^{\tau}\frac{d\sigma}{\sigma^2}\sum_{k=1}^{m}k\sum_{l=1}^{m}l\,e^{-\frac{\frac{k^2+l^2}{m^2}}{4\sigma^2}}I_0\left(\frac{kl}{2m^2\sigma^2}\right)$. The temperature (*T*) is recorded as a function of time. One all the parameters are known, the device solves for the unknown parameter: the thermal conductivity.

$$T=\frac{P_0}{\Pi^{\frac{3}{2}}ak}D(\tau) \qquad (1)$$

$D(\tau)$ is dimensionless time function.

a *: effective radius*

k : thermal conductivity

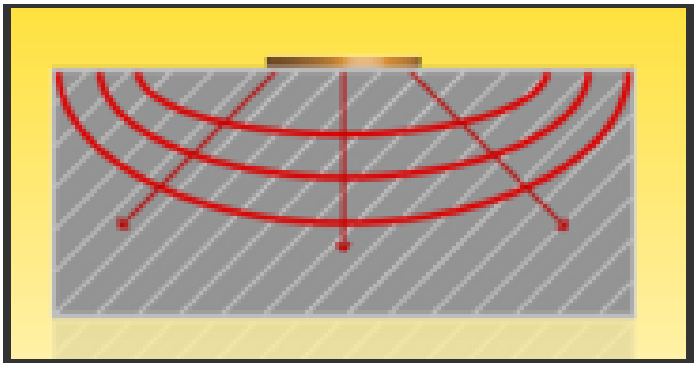

Figure 6 Heat transfer in a single sided sample

Settings | **Numeric Results**

	Status	Description	Heating Power	Measurement Time	Thermal Condu...	Thermal Diffusi...
	Calculated	acrylic_9	10 mW	40s	0.2573 W/mK	0.1529 mm²/s
	Calculated	acrylic_10	10 mW	40s	0.2593 W/mK	0.1542 mm²/s
	Calculated	Delrin_1	15 mW	40s	0.4607 W/mK	0.2246 mm²/s
	Calculated	Delrin_2	15 mW	40s	0.4607 W/mK	0.2275 mm²/s

Figure 7 Results from TPS measurements

There are many other sophisticated devices available in the market that are used to determine the thermal conductivity of materials. One other such device is the Fox 50. The set-up is shown in Figure 8.

The Fox50 indirectly measures thermal conductivity by determining the resistance of the sample. One other difference in comparison to TPS is that the Fox50 uses a steady

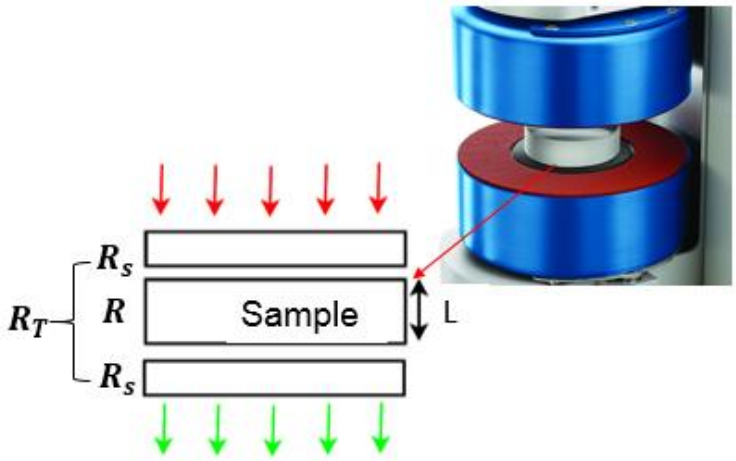

Figure 8 Fox 50 schematic and image

state two sample method. There is no single sample method as is in the TPS. The Fox50 assumes the contact resistance between the two ends of the samples and the equipment surface to be the same for the two different samples used in this method.

Total Thermal Resistance is given by

$$R_T = \frac{\Delta T}{Q} \; ; \tag{2}$$

Where, ΔT : Temperature difference

Q : Supplied Heat

The total resistance is the sum of sample resistance and the contact resistances given by:

$$R_T = 2R_s + R$$

Thermal Resistance (R) of each sample is given by:

$$R = \frac{L}{k} \tag{3}$$

Where, *L*: Thickness of the sample

k: Thermal conductivity

Now to determine the thermal conductivity of the sample material, the difference in the total resistances of the two samples of different thickness L is computed. Assuming same thermal contact resistance for two different thickness samples

$$R_{L_1} - R_{L_2} = \frac{L_1 - L_2}{k} \tag{4}$$

As '*k'* is the only unknown in equation (4), by making '*k'* the subject of the equation, one can easily find the thermal conductivity of the material.

One other such method is the LFA, Laser Flash Analysis. Here an instantaneous laser light is the heat source that provides a heat pulse on one end of the sample. An IR camera records the temperature at the other end of the sample. Using Fourier's law the thermal conductivity of the material is then computed.

Difficulty posed by curved bodies

It is to be noticed how varied equipment are built for planar surfaced bodies. However, it is an increasingly challenging task to do the same over a surface with curvature. This problem is posed by the nature of heat flow in say a cylinder. To determine the radial thermal conductivity, one cannot simply apply a variation of the Fourier's law as heat flow is not just in the radial direction but also in the *theta* angular direction and the axial direction along the height of a cylinder. This is addressed in a few papers one such very insightful paper is by *Drake. et.al,.*

Chapter 4

Experimental Evidence –non negligible heat losses

On detailed studying of the paper [1], *Drake, et, al.*, on scrutinizing the assumptions made in this publication, experimental evidence proving the assumption to be invalid were attained. This has therefore built a premise for this thesis work.

In this paper [1] the author suggests a simple methodology. An analytical model is built based on the assumption that all the heat generated by the heater coil is transmitted into the cylindrical body, perhaps because the setup is placed in vacuum and the sample is insulated. However, by a simple addition of a Heat flux sensor on the sample surface the heat flux going into the sample was recorded.

The plot in Figure 10(a), clearly shows the ingoing Heat flux is a function of time (blue solid line) and not a constant as expected (black :). A simple set up as shown in the schematic below in Figure 9(a) was used to validate the assumption of negligible heat loss made in paper [1] . The heat flux sensor reads the voltage across the two surfaces and the

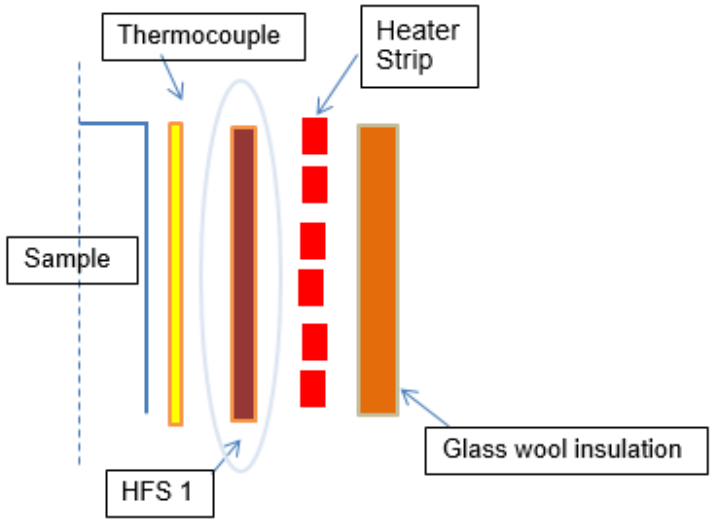

Figure 9(a) Diagram showing HFS position over a sample being heated by a heater coil

voltage can then be converted into heat flux based on the instructions that come with the sensor. The schematic highlights the position of the heat flux sensor, labeled ‘HFS 1’ between the heater coil and the sample body. The thermocouple records the temperature growth on heating with time.The data is recoded using LabVIEW VI that conveniently log the tracked data into an assigned excel sheet. On plotting this logged data we see that clearly heat flux going into the sample body is a function of time.

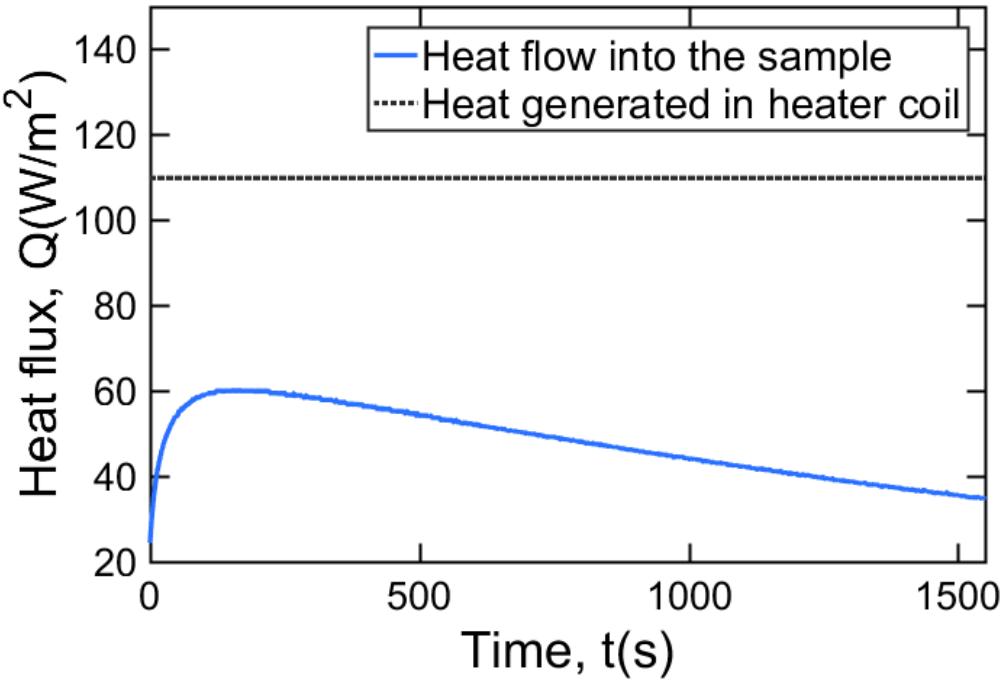

Figure 10(a) Experimental evidence showing heat going into the sample

By placing another heat flux sensor on the outward side of the heater coil the heat lost into the insulation was determined. The schematic in Figure 9(b) highlights the second heat flux sensor in the schematic and is labeled ‘HFS 2’. The plot shown below in Figure 10(b), clearly shows the heat going into the

sample(blue -), the heat lost into the insulation(red --), the heat generated in the heater coil :no heat loss assumption, (black :) and the total heat i.e the sum of heat going into the sample and out of the sample. Blue + red data. (Green curve.-).

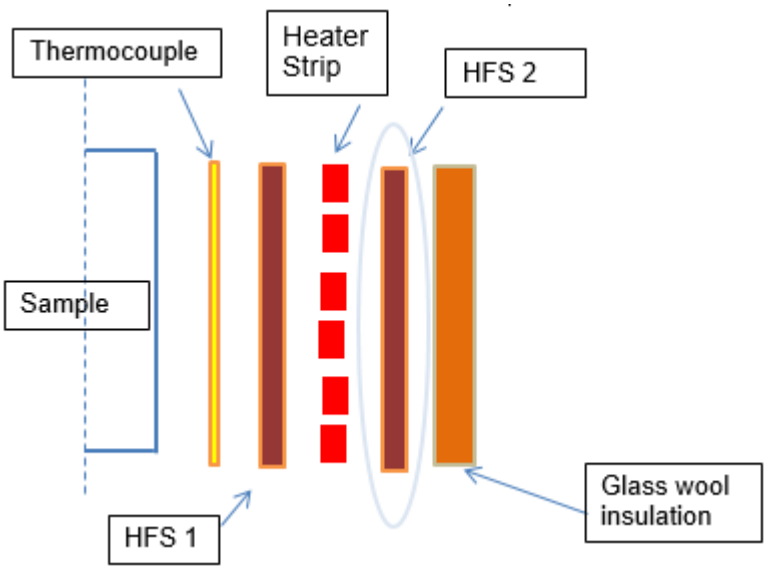

Figure 9(b) Diagram showing HFS position to record heat lost as a function of time

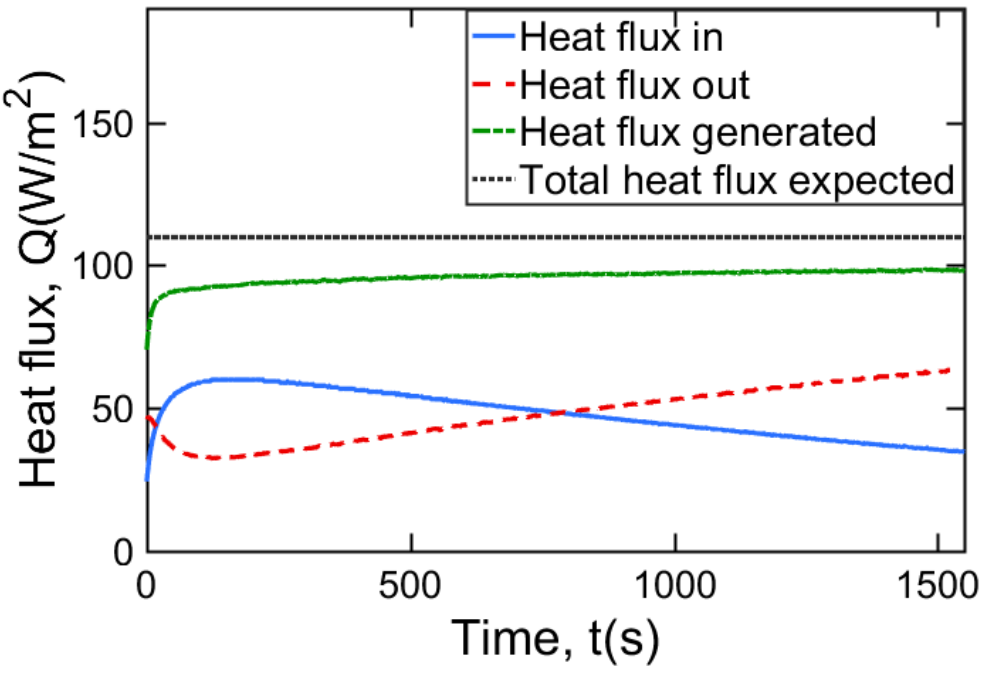

Figure 10(b) Experimental evidence showing heat going into the sample

This consolidates that the assumption: heat losses are negligible, is not true. And such a model built on the said assumption, cannot be validated using an experimental data that is generated where in heat flux is actually a function of time. A need for a model with heat flux varying with time is essential that may be validated with experimental data, hence the model and data will be in reasonable correspondence.

Chapter 5

Analytical Model for heat flux varying with time boundary condition

We have developed an analytical model that captures the effect of time-varying heat flux, *Q(t)*. By doing so, the model is able to predict the temperature rise using assumptions that are more in-line with experimental conditions.

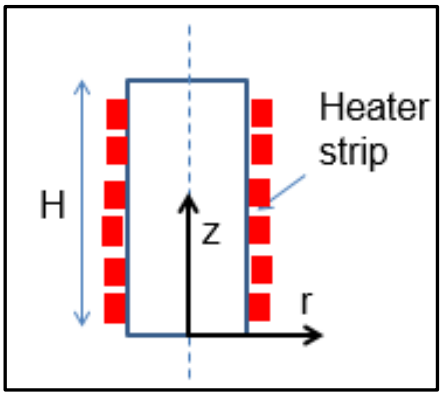

Figure 11 Coordinate axis schematic

The governing energy equation for a cylindrical body is given as:

$$\frac{1}{r}\frac{d}{dr}\left(r\frac{dT}{dr}\right)=\frac{1}{\alpha}\frac{dT}{dt} \qquad (1)$$

The boundary conditions expressed as:

$$\frac{dT}{dr}=0 \quad ;at\ r=0 \qquad (2)$$

$$\frac{dT}{dr}=\frac{Q(t)}{k_r} \quad ;at\ r=R \qquad (3)$$

Initial Condition:

$$T = 0 \qquad ; at \quad t = 0 \tag{4}$$

Let the temperature be defined as:

$$T(r,t) = \frac{2}{\rho C_p R}\int_0^t Q(t)d\tau + \theta(r,t) \tag{5}$$

Using Separation of Parameters method:

$$\theta(r,t) = \sum C_n(t) J_0(\lambda_n r) \tag{6}$$

Now solving *θ(r,t)* problem:

$$\frac{1}{r}\frac{d}{dr}\left(r\frac{d\theta}{dr}\right) - \frac{2Q(t)}{k_r R} = \frac{1}{\alpha}\frac{d\theta}{dt} \tag{7}$$

Boundary conditions:

$$\frac{d\theta}{dr} = \frac{Q(t)}{k_r} \quad ; at\ r = R \tag{8}$$

$$\frac{d\theta}{dr} = 0 \quad ; at\ r = 0 \tag{9}$$

Initial condition:

$$\theta = 0 \qquad ; at \quad t = 0 \tag{10}$$

Where λ_n are roots of the equation $J_0'(\lambda_n R) = 0$

Applying the rule of orthogonality:

$$C_n(t) = \frac{1}{N_n}\int_0^r \theta(r,t) r J_0(\lambda_n r) dr \tag{11}$$

Applying boundary conditions:

$$C_n'(t) + \alpha_r \lambda_n{}^2 C_n(t) = \frac{\alpha_r R J_0(\lambda_n R)}{N_n} \frac{Q(t)}{k_r} \tag{12}$$

Recognizing the equation is of the form:

$$C_n{}'(t) + C_n p = q(t) \tag{13}$$

Solution of such differential equation is of the form:

$$C_n(t) = \int_0^t q(\tau) e^{(-p(t-\tau))} d\tau \tag{14}$$

Therefore we now have:

$$C_n(t) = \frac{\alpha_r R J_0(\lambda_n r)}{N_n k_r} \int_0^t Q(\tau) e^{-\alpha \lambda n^{2}(t-\tau)} d\tau \tag{15}$$

Replacing *θ(r,t)* in *T(r,t),*

$$T(r,t) = \frac{2}{\rho C_p R} \int_0^t Q(t) d\tau + \sum_{n=1}^{\infty} C_n(t) J_0(\lambda_n r) \tag{16}$$

Substituting $C_n(t)$ in the above equation we have an expression for *T(r,t):*

$$T(r,t) = \frac{2}{\rho C_p R} \int_0^t Q(\tau) d\tau + \{\sum_{n=1}^{\infty} \frac{\alpha_r R J_0(\lambda_n r)}{N_n k_r} \int_0^t Q(\tau) e^{(-\alpha \lambda_n{}^2 (t-\tau))} d\tau\} J_0(\lambda_n r) \tag{17}$$

Special Case of *Q(t):*

When the heat flux varying with time *Q (t),* is replaced by a constant heat flux Q_0 the solution now changes to:

$$T(r,t) = \frac{2Q_0 t}{\rho C_p R} + \frac{2Q_0 R}{k_r} \sum_{n=1}^{\infty} \frac{J_0(\lambda_n r)}{(\lambda_n R)^2 J_0(\lambda_n R)} - \frac{2Q_0 R}{k_r} \sum_{n=1}^{\infty} \frac{J_0(\lambda_n r)}{(\lambda_n R)^2 J_0(\lambda_n R)} \exp(-\alpha_r \lambda_n{}^2 t)$$

(18)

This is now compared to the result from [1] which is printed below:

$$T(r,t) = \frac{2Q_0 t}{\rho C_p R} + \frac{Q_0}{k_r R}\left[\frac{r^2}{2} - \frac{R^2}{4}\right] - \frac{2Q_0 R}{k_r}\sum_{n=1}^{\infty}\frac{J_0(\lambda_n r)}{(\lambda_n R)^2 J_0(\lambda_n R)}\exp\left(-\alpha_r \lambda_n{}^2 t\right) \qquad (19)$$

From paper [1].

On comparison the first and the last terms of the two equations (18) and (19) are exactly the same. The second term are clearly different from one another. On evaluating these expressions, for the same *r,* k_r and *R* values, the expressions provide the same result. This helps us conclude that the expressions essentially bare the same meaning. And hence, when $Q(t)=Q_0$, i.e, when heat flux is not changing with time, the resultant solution transcends into the expression from paper [1]. This means that Q_0 constant heat flux boundary condition is only a special case of heat flux varying with time *Q(t)* boundary condition.

This suggests that if one would enforce a Q_0 heat flux boundary condition experimentally, it may then be used to validate Q_0 analytical model data. This maybe done using the LabVIEW VI which helps us define the ingoing heat flux and monitor the current value to make changes if necessary. The two experiments one with *Q(t),* i.e., heat flux varying with time boundary condition , and the other with Q_0, heat flux a constant boundary condition ; and their appropriate corresponding experiments are used to validate these models.

The LabVIEW VI code is very alike Simulink of MATLAB, the following show images of the user interface and block diagram panned images.

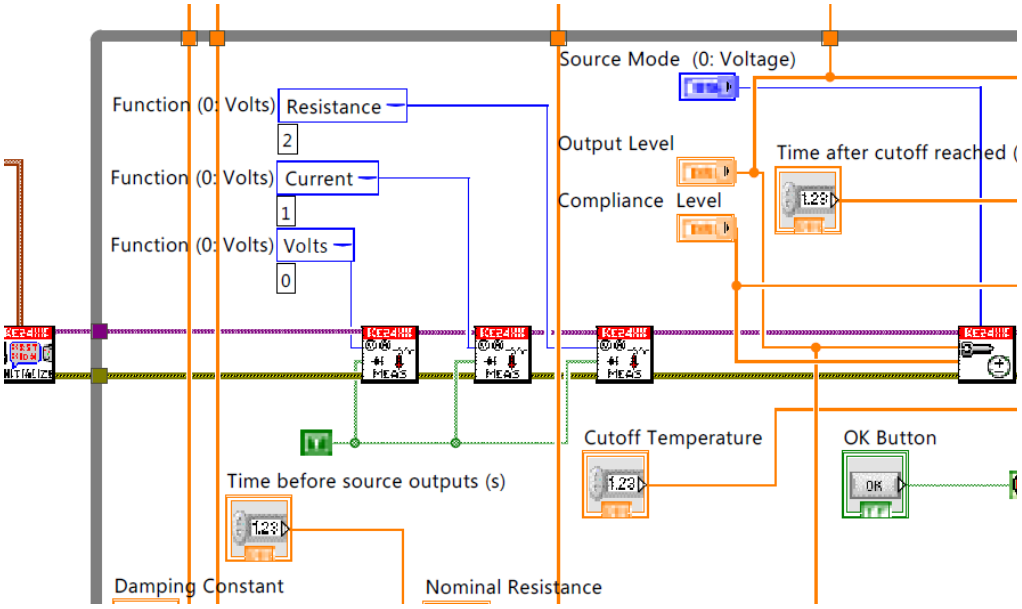

Figure 12(a): LabVIEW block diagram-panned

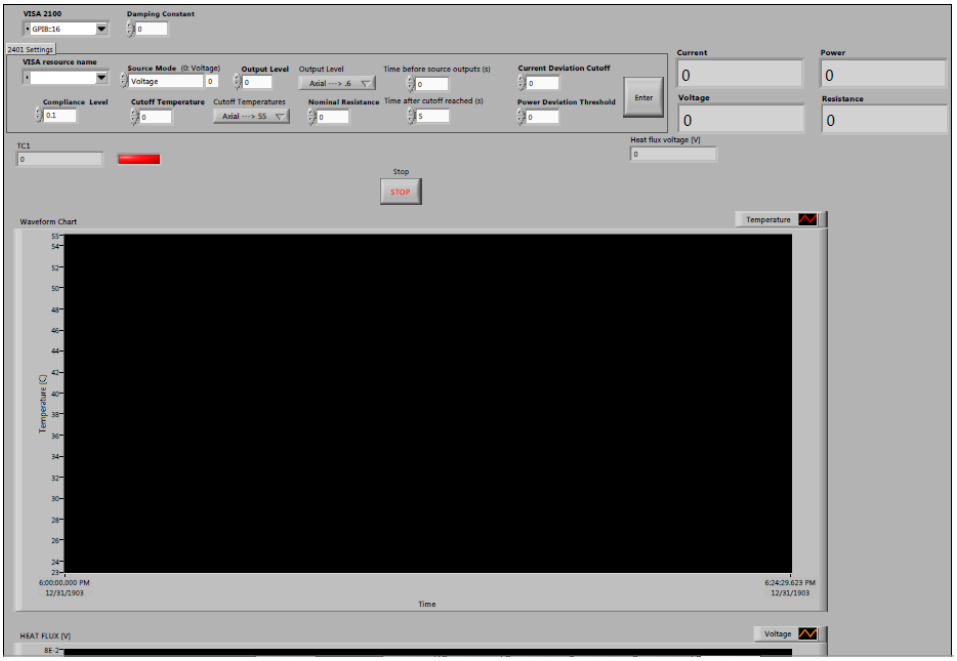

Figure 12-b LabVIEW user interface

Chapter 6

Model- Experiment correlation

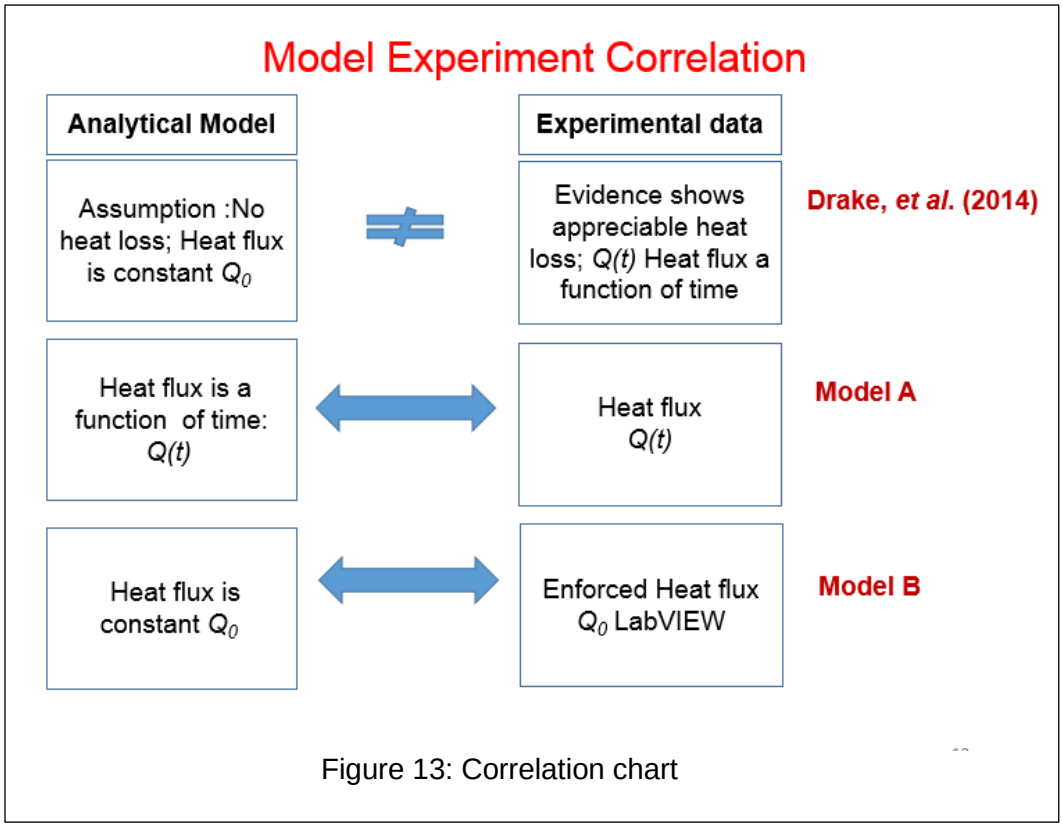

Figure 13: Correlation chart

The correlation chart shows that by building experimental set up more in-line with the model boundary conditions and assumptions one is able to validate the model and determine reasonable results more appropriately. Attempting to validate a model with an experiment with no correlation between them will lead to erroneous results. As experimental data suggests that heat loss in in fact a non-negligible quantity the model then validated using an experiment with appreciable heat loss in *Drake.et.al.,* is highlighted.

Therefore a model as discussed before was built to account for the heat loss and this is then validated with the experimental set up where in heat loss is large: Denoted by Model-A in the chart.

By enforcing a constant heat flux on the surface of the sample in another experiment we can make another set of model-experiment that correspond to each other. This is shown as Model B in the correlation chart. The model for this case is discussed in the Special case of Chapter 4.

Before subjecting a Li-ion cell to these, the experiment-model are first tested on well-known standard materials like Acrylic and Delrin. These materials have the same geometrical shape as the Li-ion cell denoted by the number 26650. 26 denotes the diametric dimension of the cylinder in mm and 650 denotes the height of the cylinder in mm units.

Chapter 7

Experimental set up

An experimental technique for determining the anisotropic radial thermal conductivity and heat capacity of the cylindrical body was developed in this work. The experimental data was used to validate the analytical model. The cylindrical body true to the boundary conditions used in the model was subjected to adiabatic heating varying with time at r=R surface condition. A nichrome heater coil is used to provide the necessary heat flux. The temperature rise of the cell surface is monitored using a T-type thermocouple. A heat flux sensor was used to determine the heat flux entering the sample body at the surface at r=R. Fiber glass wool insulation was use to insulate the sample and minimize heat loss. All experiments are carried out in Vacuum to further reduce heat loss.

A schematic of the sample preparation is shown in Figure 14(a) ,(b) below. The sample is wrapped with multiple layers. Each layer has its very own importance. First the sample is measured and checked for the dimensions. The dimensions of all specimen is established by the number 26650: 26 mm diameter, and 650 mm in height of the cylinder. This is then electrically insulated using kapton electric insulation, this ensures that the battery is safe from short circuiting while experiments being conducted. A T-type thermocouple is then placed at the center height level of the cylinder at the surface r=R. This thermocouple is secured in place using kapton tape. A heat flux sensor is then placed over the thermocouple so the ingoing heat may be recorded, this like the thermocouple is positioned using kapton tape. Next is the steel foil, this ensures that heating is uniform over the curved surface of the cylinder. Another layer of tape to keep the foil from sliding off. Then a heater coil is wound over the cylindrical body, maintaining equally spaced windings. Finally the sample is enclosed in glass wool insulation and once the Heat flux sensor,

thermocouple and heater coil terminal connections the sample is placed in vacuum and sealed to a low pressure of - 45 kPa (gage) vacuum.

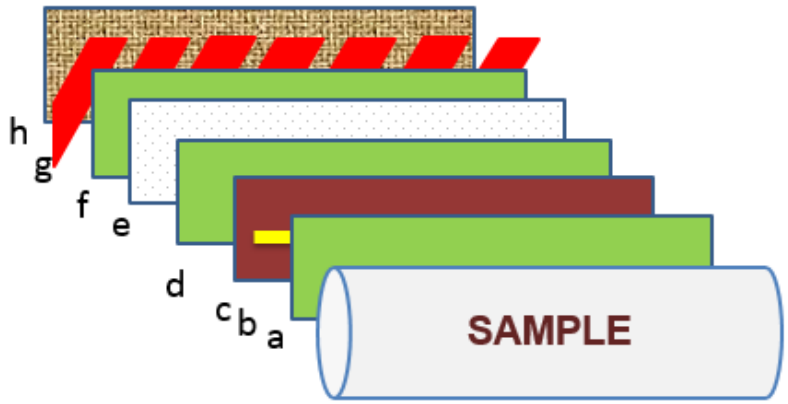

Figure 14(a) Schematic of sample preparation

Figure 14(b) Images of sample preparation steps.

a, d, f, g: Kapton tape (Electric Insulation)
2, b: Thermocouple (Record Temperature of the sample at r=R)
3, c: Heat Flux Sensor (Record Heat going into the sample)
4, e: Steel Foil (Ensure uniform heat supply at the surface)
5, g: Heater strip (Heat source)
6, h: GlassWool insulation (heat Insulation)

A Keithley 2401A sourcemeter is used for supplying heating current and keithley 2100A multimeter is used for measuring voltage across the heater coil. The thermocouple output is sampled at 2 Hz using a National Instruments (NI) 9213 24-bit thermocouple module within an NI cDAQ-9213. Data acquisition is controlled using NI LabVIEW software. Electrical resistance of nichrome heaters used in this work is measured at room (around 23℃) temperature. A schematic of the connections for the experimental set up is shown

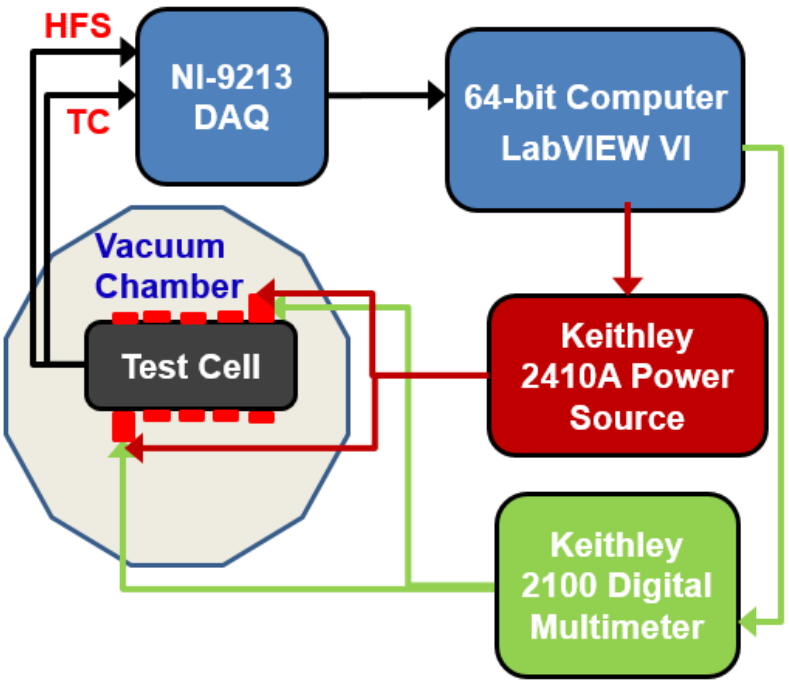

Figure 15(a) Block diagram of experimental set up

below in Figure 15(a). An image of the in house built vacuum set up is also shown in Figure 15(b).

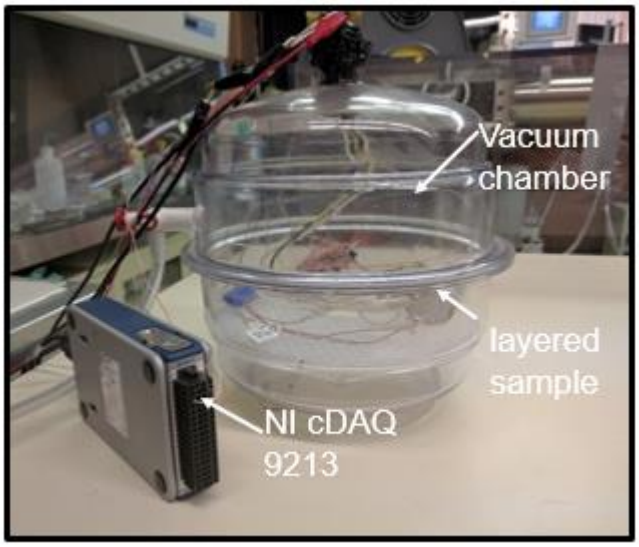

Figure 15(b) In house built vacuum chamber

The LabVIEW VI is used to monitor ingoing current, the power and duration time of the experiment. It also provides for a visual plot of the temperature growth with time and Heat flux varying with time recorded by the thermocouple and heat flux sensor in real time. The recorded data is then saved in the form of an excel file, the data is used to validate the model temperature prediction. The temperature curve generated by the analytical model in the MATLAB code needs a value for thermal conductivity and heat capacity, by trial and error multiple combinations are tried out which result in a certain temperature profile. When this profile overlaps with that of the experimental data it is believed that the (k_r, C_p) used for the computation of the analytical model are the same as that of the cylindrical material

used to carry out the experiments. This was the method implemented by the paper in discussion, called as curve fitting. But on further data analysis it was understood that the curve fit is largely sensitive to changes in C_p , but not so much for change in k_r. Also because two parameters are in play, that decide the temperature profile, one can achieve more than just one combination set of these parameters that may satisfy the curve fit. For example on holding a certain k_r value and changing C_p one can achieve a k_r,C_p combination and may get a different set of solution combination if C_p was held constant and *kr* was changed until a good fit was attained. Hence a detailed study of these short comings was necessary to provide more robust solutions.

Chapter 8

Analysis of experimental and analytical data

To overcome the drawbacks of plain trail error curve fitting as discussed in the previous chapter; a code was built to calculate the error or deviation between the experimental curve and the analytical model curve for a range of different combinations of k_r, C_p using the method of least squares. A color plot was then generated to determine the minima of deviation which corresponds to a certain k_r, C_p combination. This consolidated that the analytical model curve is more sensitive to changes in C_p, than it is to changes in *kr*. Refer figure 16(a).

To recheck the color plot more plots were created. The best fit suggested by the color plot curve, a curve with best fit C_p and a k_r*(new)*=best fit k_r±20%(best fit k_r value); Similarly, best fit k_r and C_p*(new)*=best fit C_p ±20%(best fit C_p*)*, hence 5 of these curve were plotted. And this confirmed that the curve fit is largely sensitive to C_p changes and not k_r. Refer Figure 16(b).

To recheck the color plot results more studies on parameter sensitivity were conducted. Another issue was lack of repeatability for experiments. One recent paper that brought sensitivity of parameters and optimal experiment design solutions was that of Jason Oztanek's paper [2] on sensitivity analysis.

A detailed study of the paper titled of paper [2] gives necessary insight on the Design of Experiments and the parameter sensitivity through a sensitivity test called 'D-Optimality'.

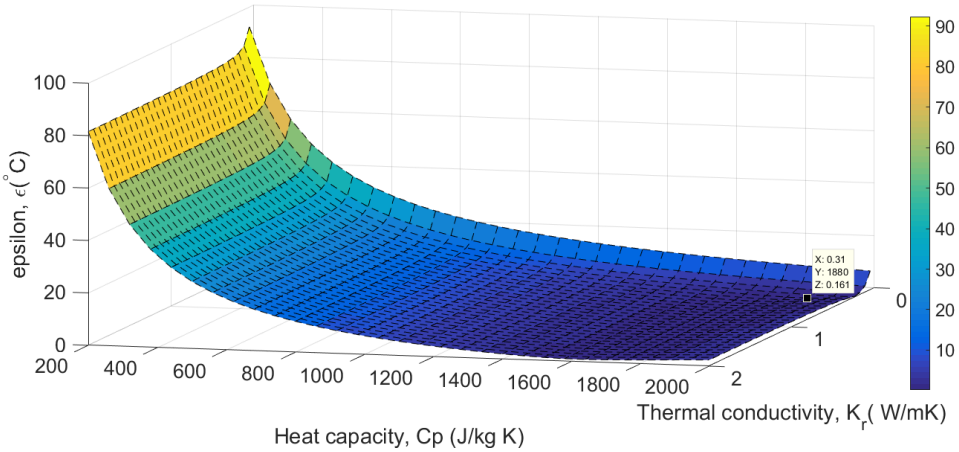

Figure 16(a) Color plot

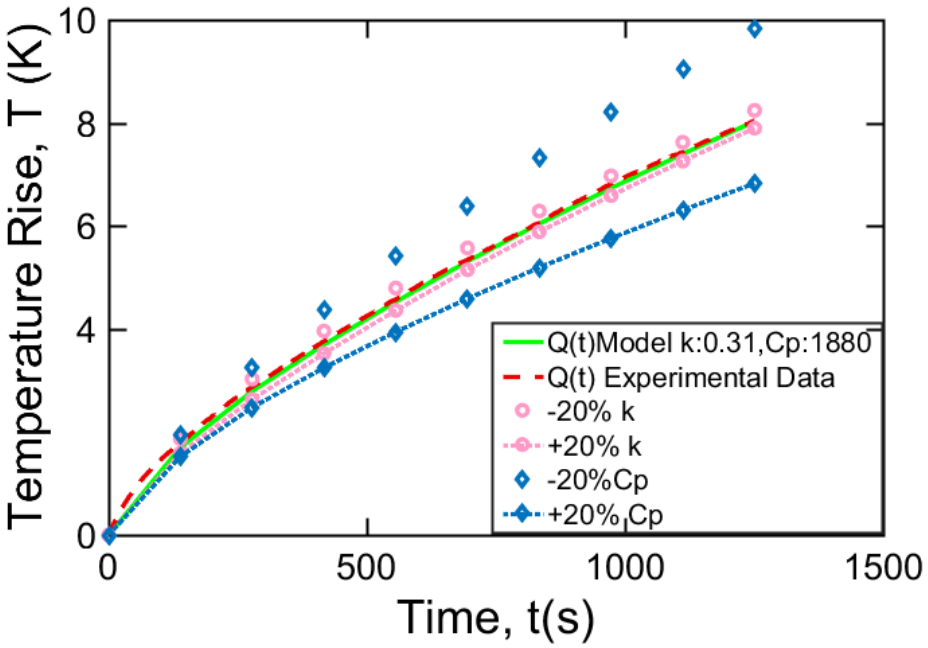

Figure 16(b) Sensitivity test

D-Optimality criterion

D-Optimality is a way of optimizing the design variables of an experiment so as to minimize the variance associated with the parameters. This is a well-known sensitivity test used to determine sensitivity of desired parameters in cases such as actuator, initiators, detonators and air bags. It is used to maximize our knowledge of the parameters of interest. D-Optimality is however a function of the chosen sample population distribution. This important parameter was determined as is in the paper cited above [2].

$$\Delta_1^{+} = \frac{1}{\tau}\int_0^{\tau} (X^{+})^2 (\theta_m)^{-2} d\tau' \tag{1}$$

$$X^{+} = \left(\frac{\beta}{\theta_m}\right)\frac{d\theta_m}{d\beta} \tag{2}$$

$$\theta_m{}^{+} = \frac{\overline{\theta(\tau)}}{\theta_{nom}} \tag{3}$$

$$C_{ij}^{+} = \frac{1}{\tau}\int_0^{\tau} (X_i{}^{+} X_j{}^{+})(\theta_m)^{-2} d\tau' \tag{4}$$

$$\Delta_2^{+} = C_{11}^{+} C_{22}^{+} - (C_{12}^{+})^2 \tag{5}$$

Δ_1^{+} is the D-optimality criterion for single parameter

Δ_2^{+} is the D-optimality criterion for two parameter

τ is the experiment duration

β is the non-dimensional sensitivity coefficient, and

θ_m is the maximum temperature rise.

Cij$^+$ is the determinant of the cumulative sensitivity coefficient matrix

In Eq. (2) β is the parameter of interest, θ_{nom} is the nominal temperature rise. From Eq. (3) $\theta_m{}^+$ is a function of τ, the limit of integration in (1) and not the integration variable, τ'.Δ_1^+ provides the optimality criterion for a single-parameter, nonlinear model. Maximizing Δ_1^+will minimize the variance in the estimated parameter. The optimal duration of the experiment would be the time τ, at which Δ_1^+ is a maximum. For the single-parameter model. The same principle is true for the two-parameter model, with the exception that the criterion is to maximize the determinant of the cumulative sensitivity coefficient matrix, Cij$^+$ where i=1 to *p* and j=1 to *p*. For the two-parameter model, the determinant of the Cij$^+$ matrix of order two is readily calculated using for Δ_2^+ . Note Eq.(4) becomes is identical to Eq.(1) (Δ_1^+) when i=j. In other words, the terms on the primary diagonal of the Cij$^+$ matrix are equivalent to the single-parameter D-optimality criterion for the *p* parameters.

D-Optimality shows the optimal length of the experiment to be chosen for the said parameter to be determined with least variance possible. This is the time length that is associated with the highest D-Optimal peak over the total time of the experiment. The higher the D-optimality for two comparable experiments, i.e, two experiments for the same parameter of interest, the least is the variance for the higher D-optimality.

The following set of plots show a D-optimality calculated for Single parameter (k_r) , and Single parameter *(C_p)* and two parameter *(k_r,C_p)*; Non Linear models to determine the optimal experimental time period to attain the parameters of interest in each case with least possible error. The plots shows below are that of Delrin material.

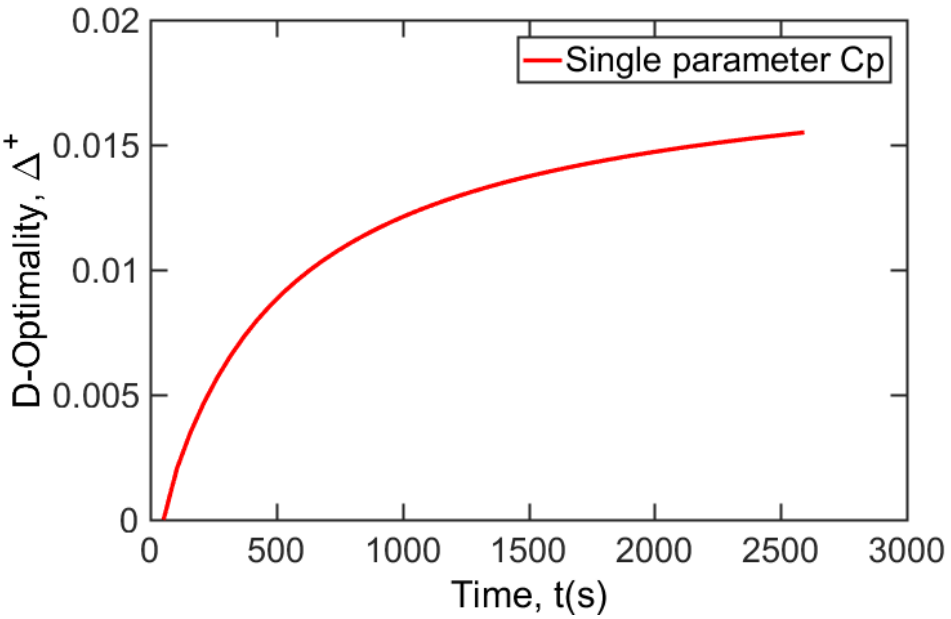

Figure 17(a) D-Optimality v/s time Single parameter (C_p) Non-linear model [*Q(t)* Delrin]

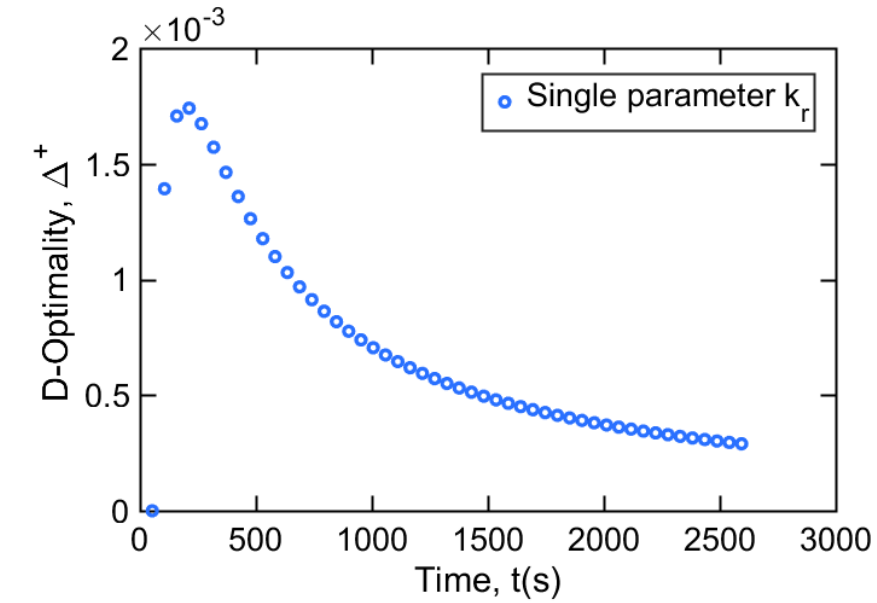

Figure 17(b) D-Optimality v/s time Single parameter (k_r) Non-linear model [*Q(t)* Delrin]..

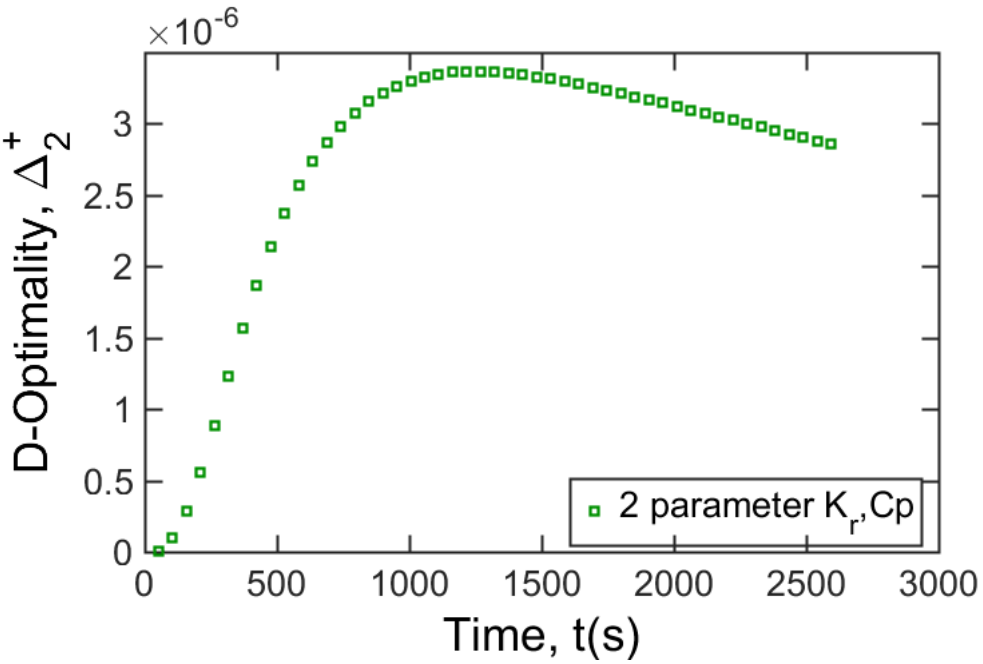

Figure 17(c) D-Optimality v/s time two parameter (k_r,C_p)
Non-linear model [$Q(t)$ Delrin]

Clearly, from the Figure 17 series, D-Optimality vs time curves, it is confirmed that the experimental set up is highly sensitive to heat capacity C_p. The Single parameter C_p curve suggests that with increase in experimental time the deviation associated with determining this heat capacity parameter through this experiment keep on decreasing i.e the possibility of attaining a lesser error in estimating this parameter increases with time. In case of the single parameter k_r curve, a clear peak is attained at 212 seconds hence the best case scenario to determine the thermal conductivity of, in this case standard material delrin, is attained at an experimental length of 212 sec. In comparison the two parameter (k_r,C_p) D-optimality (Δ^+_2) curve does not have a clear peak.

In the two parameter D-optimality (Δ^{+}_{2}) the lack of a clear peak demands for another perhaps longer experimental data set. Also to find a minima over a range of k_r, C_p combination matrix means a very long computation time is needed. The matlab code take about 40 hours of computation to determine the best fit minima combination of k_r,C_p where *kr* range is given by 0.05 to 2 W/mK and C_p range of 200 to 2000 J/kg K , in steps of 51 in each range. These long computation and no clear peak created ambiguity if this was the best method to attain the two parameters k_r, C_p through one single experiment worth it. With C_p easily available of the material, and a clear peak in single parameter k_r, attempts to find k_r alone at the d-optimal time were conducted. At this point the aim of the problem statement has shifted to finding a single parameter given the C_p of the material and the optimal experimental time at which the solution is optimized.

Therefore, after studying these interesting plots, it was decided that as determining heat capacity of a body, is, in comparison to determining the thermal conductivity over a cylindrical surface, a trivial task. The problem can be narrowed down to just attempting to determine the thermal conductivity of the body, using the heat capacity of the entity attained from Transient Planar Source Hot disk plate equipment readings or simply from a calorimetry reading.

These studies helped reinstate repeatability in determining the thermal conductivity of the material. The optimal time is determined for every sample specimen and then the computations for that time period are executed, driving the problem to one solution.

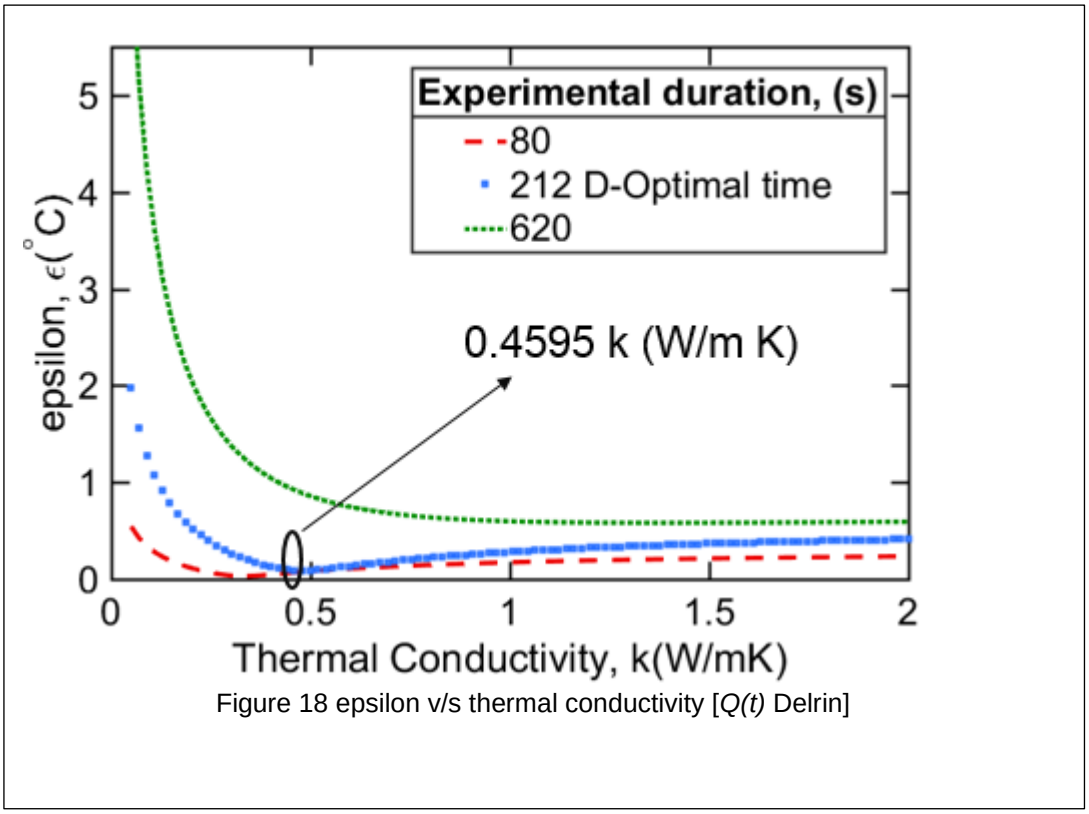

Figure 18 epsilon v/s thermal conductivity [*Q(t)* Delrin]

In Figure18 shown above the epsilon minima for a range of thermal conductivity values. The plot shows the same for different experimental time durations. The D-optimal experimental length shows a minimal error between the experimental and analytical model curve at 0.45 W/mK, and this is close to the TPS reading of the sample which is 0.46. The two other time lengths of experiments show a large deviation from the TPS readings which is the actual material property of the sample used. Hence this shows that running the experiment for a D-optimal length is essential for a least error in solution.

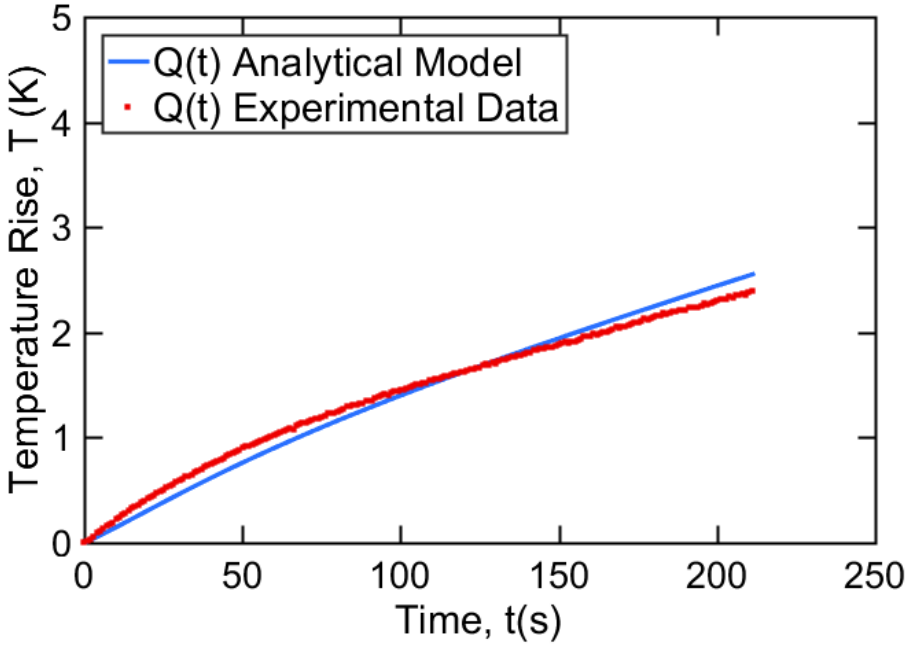

Figure 19(a) Best fit [*Q(t)* Delrin]

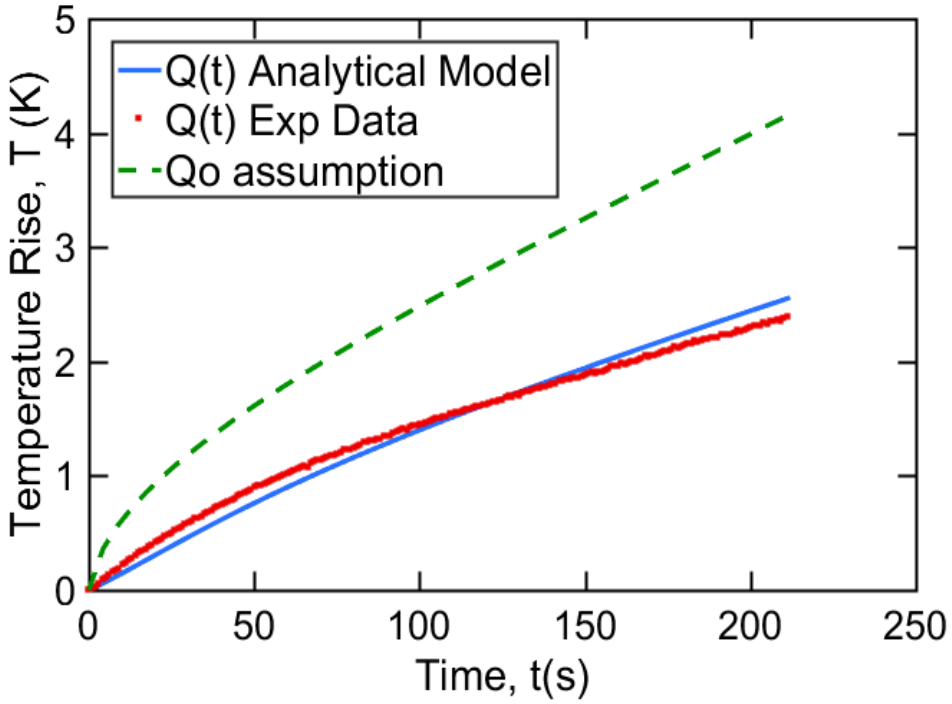

Figure 19(b) Best fit v/s Q_0-assumption

Figure 19(a) shows the best curve fit at the determined thermal conductivity. This shows a less than 0.5 deg C variation in the experimental and analytical model for heat flux varying with time boundary condition.

This plot below in Figure 19(b) shows the best fit for the determined values in comparison with the Q_0 assumption made in paper[1]. This shows that the model prediction and the experimental data are starkly different from each other as a result of model built based on wrong presumptions. This on curve fitting would predict a whole different set of *kr,Cp* from the real *kr, Cp* combination.

The experiments repeated for Q_0 model with heat flux constant boundary condition and Q_0 enforced to be constant in the experiment through LabVIEW, these experiments are referred to as Q_0 model and experiment. The following are the resultant plots.

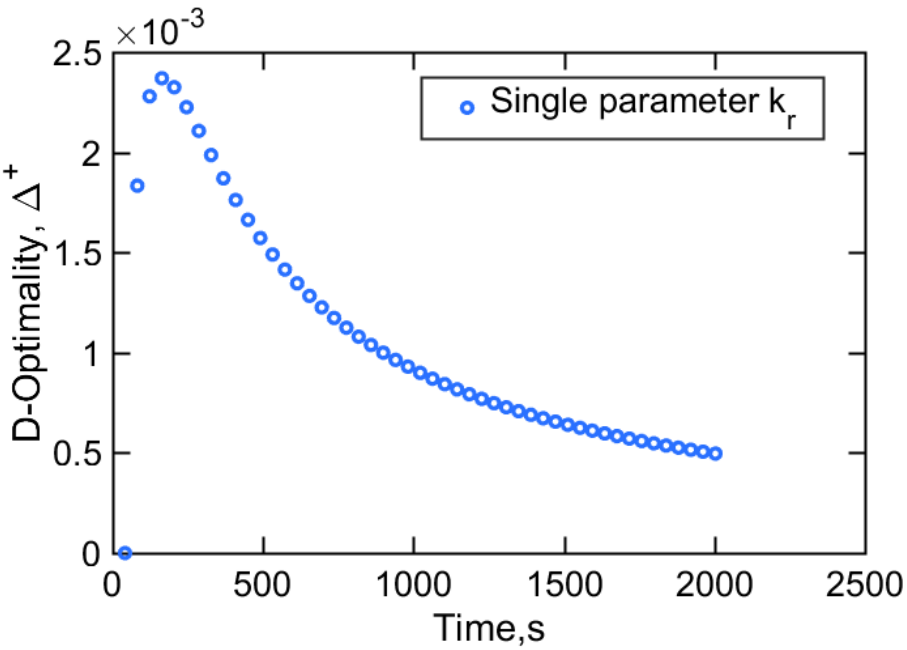

Figure 20 D-Optimality v/s time Single parameter (*kr*) Non-linear model [*Qo* Delrin]

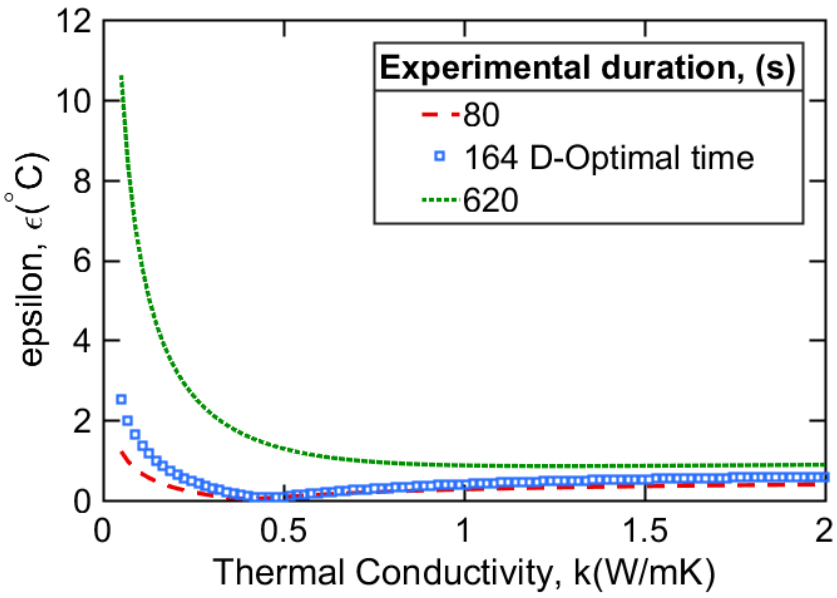

Figure 21 epsilon v/s thermal conductivity [*Qo* Delrin]

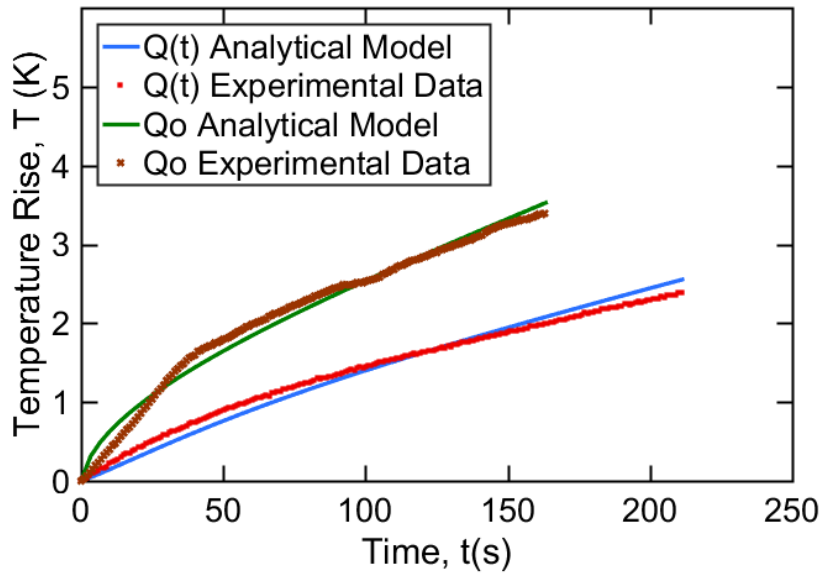

Figure 22 Best fit *Q(t)* model v/s Best fit Q_o model [Delrin]

This plot in figure 22 shows the *Q(t)* heat flux varying time experiment and model curve fit, along with Q_0 constant heat flux model and an experiment where in heat flux was forced to be a constant using LabVIEW. This shows that with more inline experiment and model correspondence the results are nearly the same. This shows that Q_0 model is true for an experiment with a true Q_0 constant heat flux entering the sample body.

Chapter 9

Results

The results are printed out in this section of thesis. The model and experimental data are validated with standard materials like acrylic and as previously shown, delrin. Then the same methodology is used to determine the effective radial thermal conductivity of a Li-ion cell. These results are then compared to S.J.Drake's paper [1]. The results are tabulated and the plots pertaining to these results are arranged in sequential order of computation.

Acrylic *Q(t)* model

D-optimal criterion is computed for the acrylic data. The peak is noted at time of 202 sec. This is shown in the plot below.

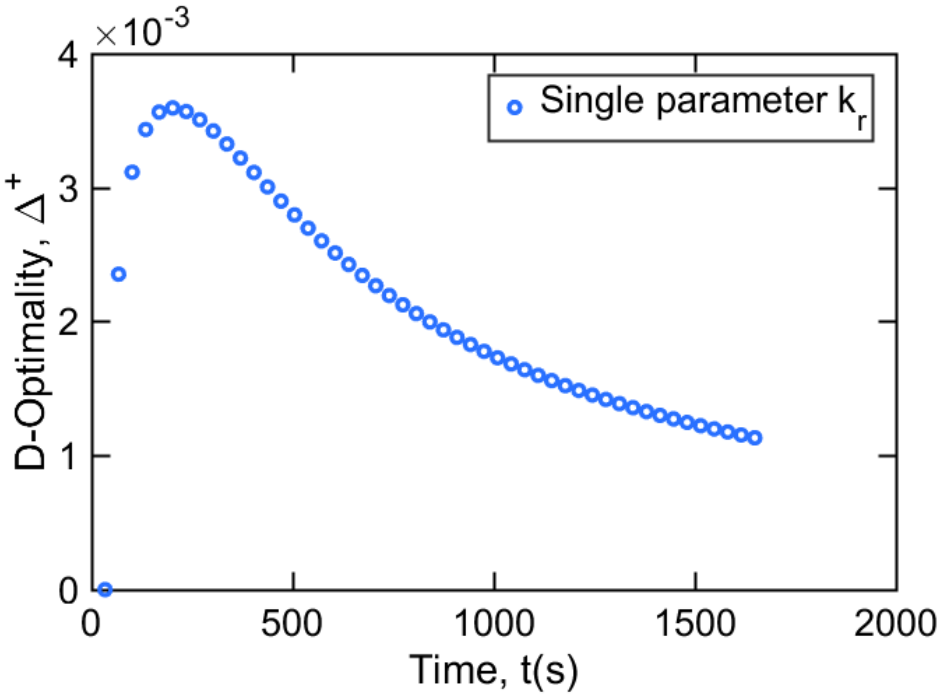

Figure 23 D-Optimality v/s time Single parameter (k_r)
Non-linear model [*Q(t)* Acrylic]

The minimum error between experimental and analytical curve is determined for a range of thermal conductivity values and the thermal conductivity for D-optimal time is found to be 0.26. This is shown in figure 24.

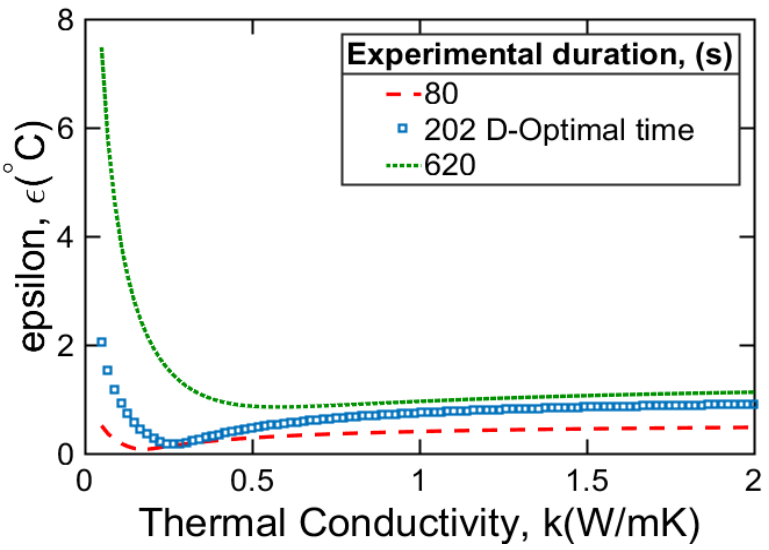

Figure 24 epsilon v/s thermal conductivity [*Q(t)* Acrylic]

This thermal conductivity is very close to the TPS standard material property value which is 0.25.The best fit is shown in figure 25(a) Now that the material property is found a best fit curve is plotted to further compare with a Q_0 assumption. Refer to Figure: 25(b).

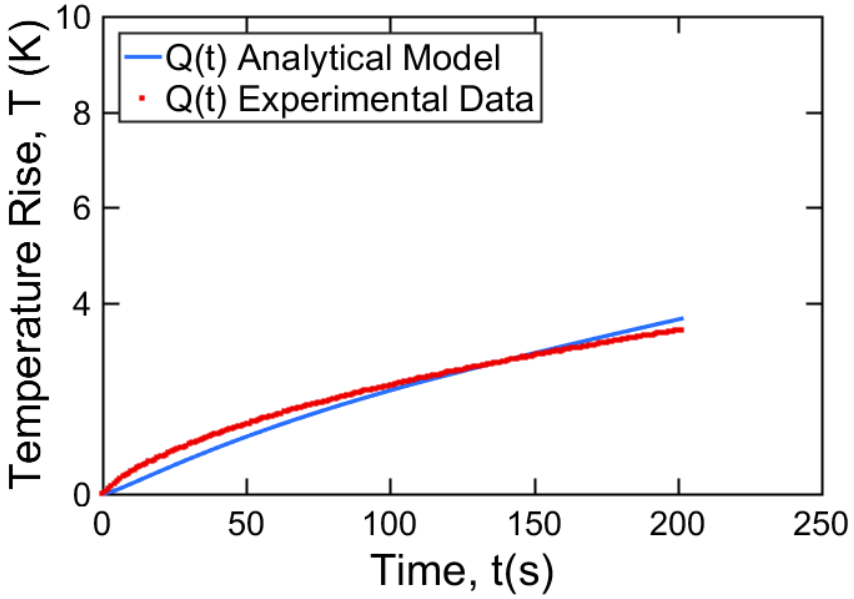

Figure 25(a) Best fit [*Q(t)* Acrylic]

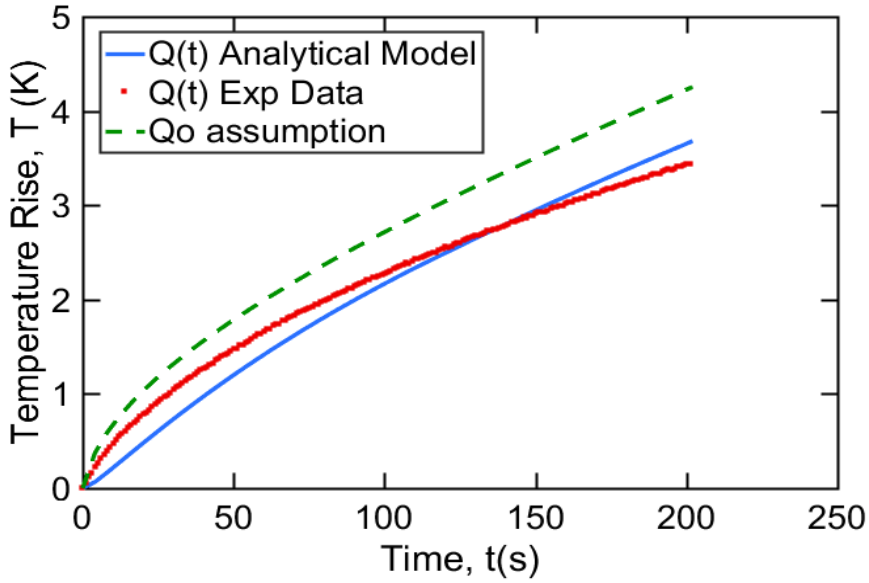

Figure 25(b) Best fit v/s Q_0-assumption [Acrylic]

Acrylic *Qo* model

Next *Qo* model and experiment with enforced constant heat flux, computations are carried out just like for *Q(t)* model and experiment data. The D-optimal peak for single parameter (*kr*) computation is found at 194 sec.

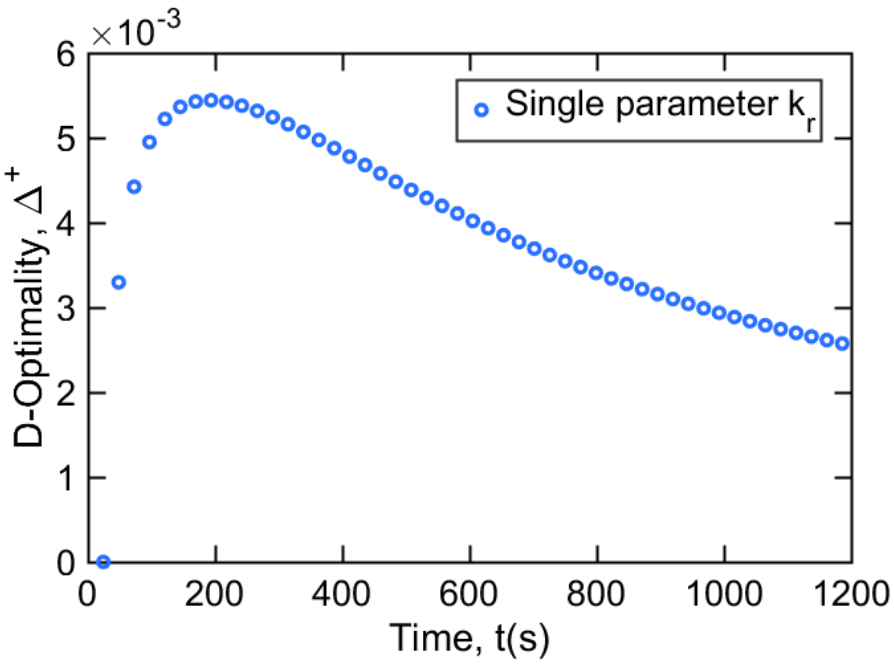

Figure 26 D-Optimality v/s time Single parameter (*kr*) Non-linear model [Q_0 Acrylic]

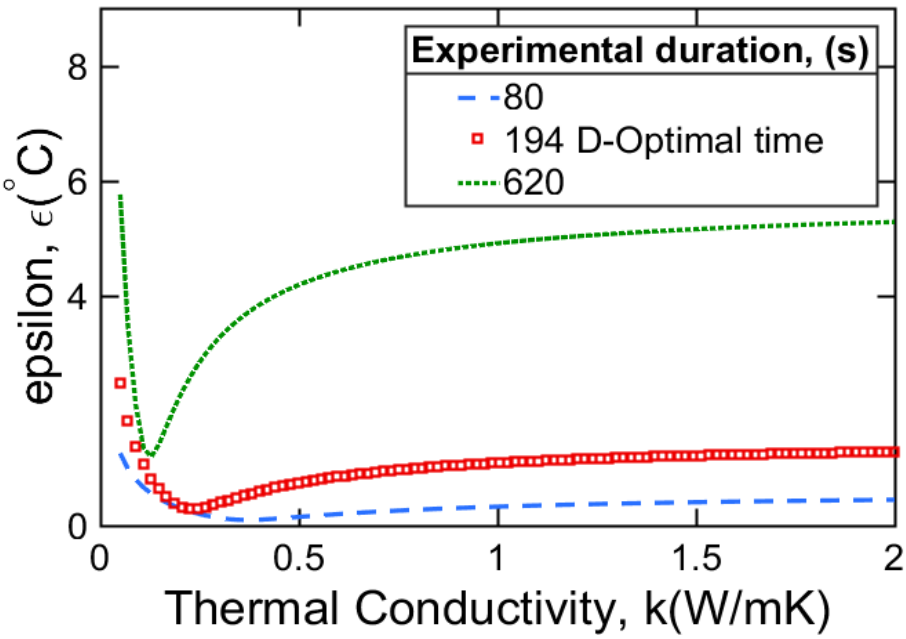

Figure 27 epsilon v/s thermal conductivity [*Qo* Acrylic]

The figure 27 shows the minima at 0.24 thermal conductivity when executed at D-optimal time length.

Finally, the *Q(t)* model and corresponding plot are compared against the *Qo* model and experiment with enforced constant heat flux. Figure 28 shows how the two models compare.

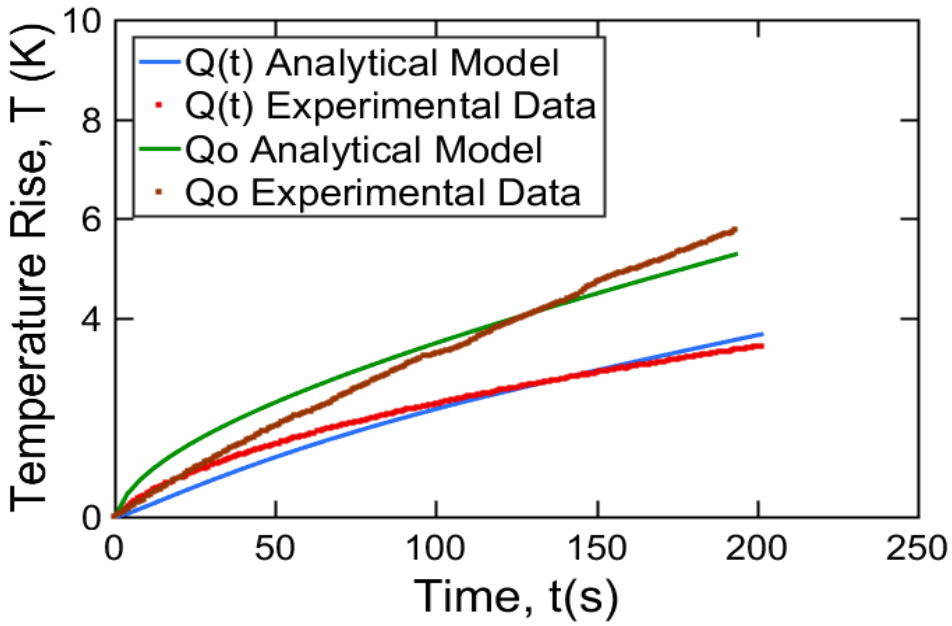

Figure 28 Best fit $Q(t)$ model v/s Best fit Q_o model [Acrylic]

Li ion *Q(t)* model

Again the same methodology is followed and the plots are printed below.

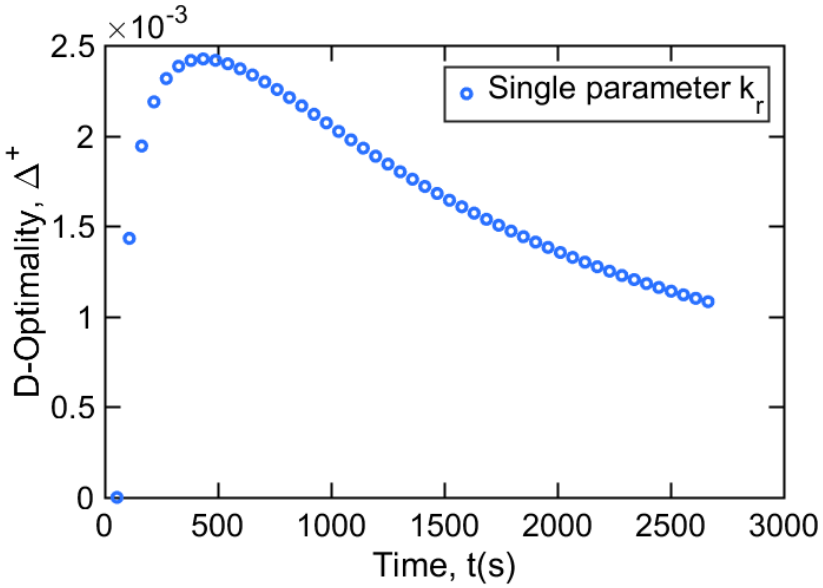

Figure 29 D-Optimality v/s time Single parameter (*kr*) Non-linear model [*Q(t)*Li-ion]

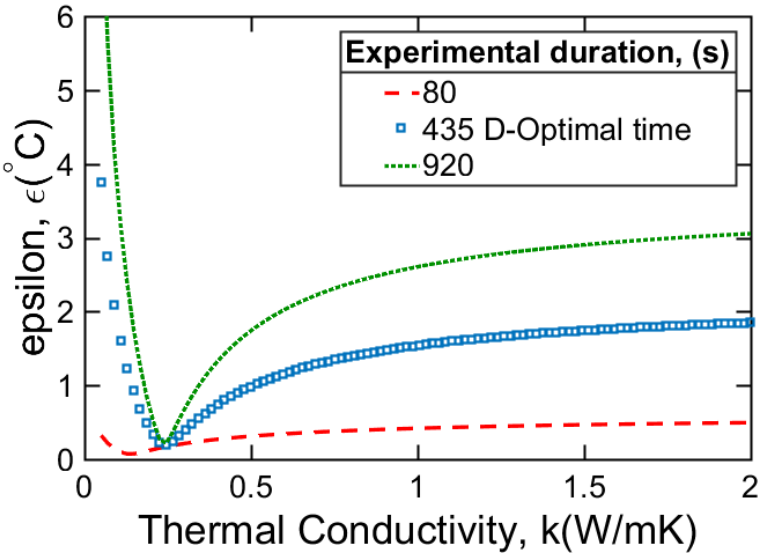

Figure 30 epsilon v/s thermal conductivity [*Q(t)*Li-ion]

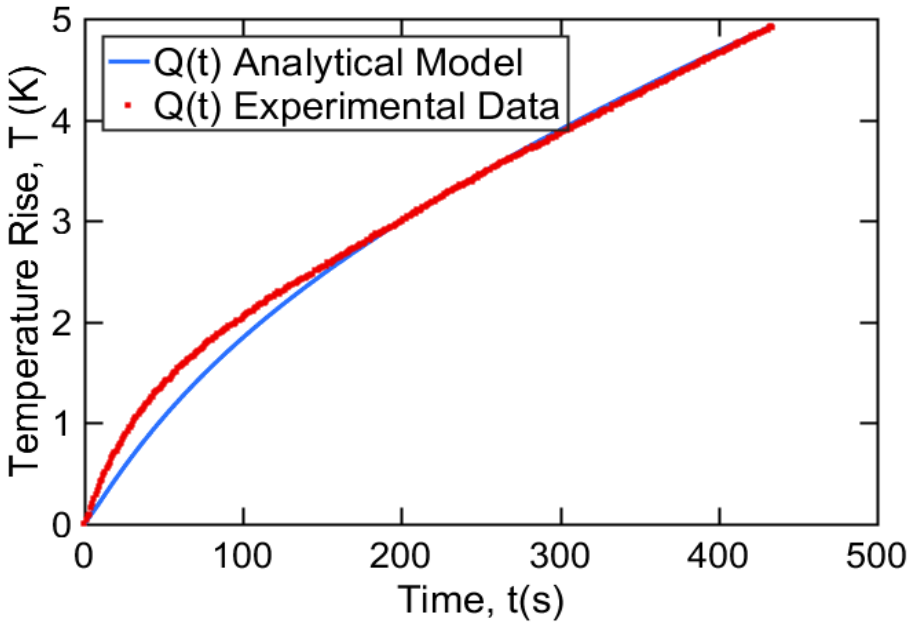

Figure 31 Best fit [*Q(t)* Li-ion]

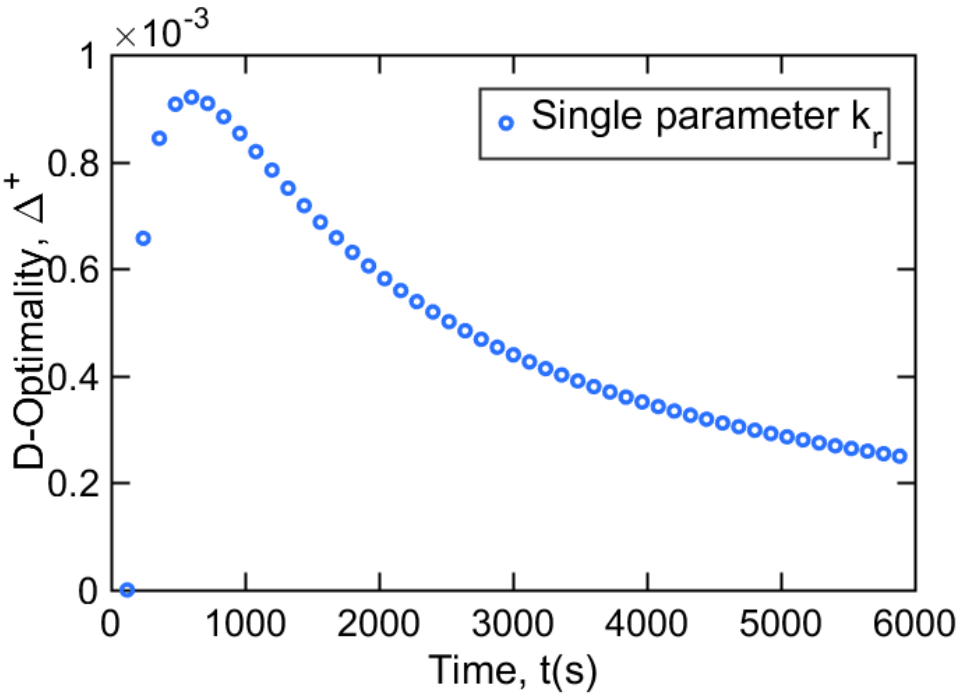

Figure 32 D-Optimality v/s time Single parameter (k_r) Non-linear model [Q_0Li-ion]

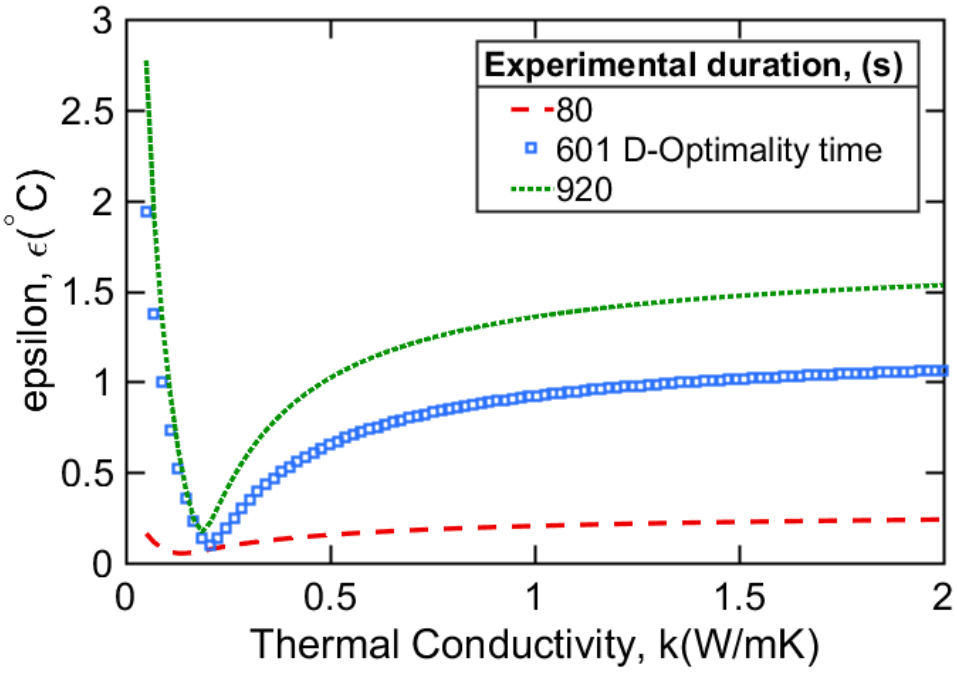

Figure 33 epsilon v/s thermal conductivity [Q_0 Li-ion]

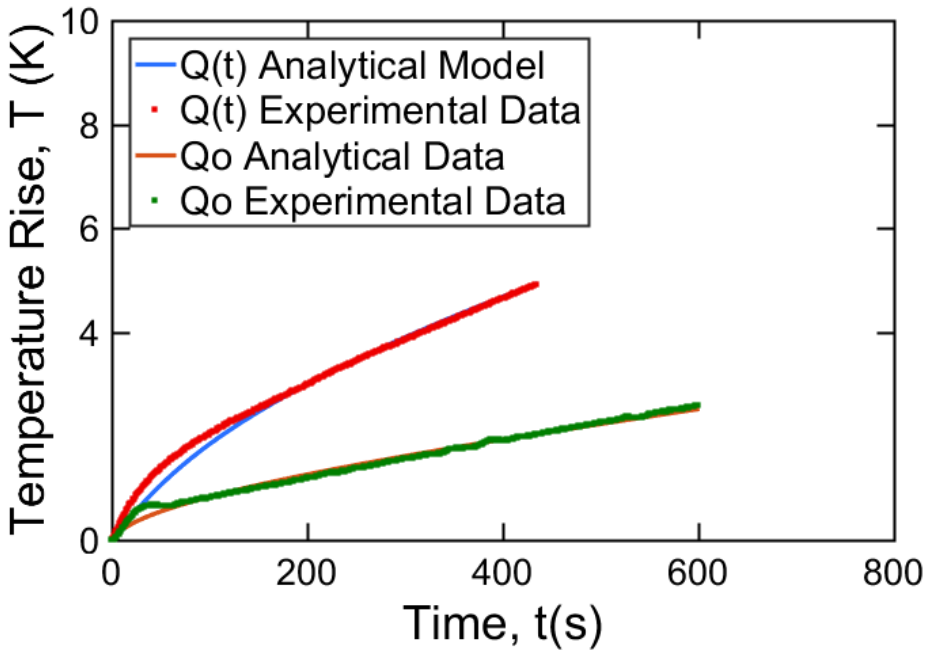

Figure 34 Best fit *Q(t)* model v/s Best fit [*Qo* model Li-ion]

TABULATED RESULTS:

Material	*Q(t)* Model	Q_0 Model	TPS Measurements	Percentage change
DELRIN	0.45	0.45	0.46	2.17
ACRYLIC	0.26	0.24	0.25	4.00
LI-ION CELL	0.24	0.20	-	-

Table 1-1 *Q(t)* , Q_o, TPS measurements comparison

Material	Average *Q(t)*,Q_0 Models [Appropriate experiments]	Assumption Q_0 paper [1]	Percentage change %
Li ion 26650	0.22	0.15	46.6

Table 1-2 comparison between improved method & paper [1] reported k values

Conclusions:

1. A generalized analytical model that accounts for heat loss is developed. The model with constant heat flux is a special case of varying heat flux *Q(t).*
2. A corrected experimental set up for constant *Qo* was built, *Qo* model was then validated against the corresponding right experiment.
3. The drawbacks associated with curve fitting were identified. Repeatability and parameter sensitivity was established through D-Optimality criterion that ascertains an optimal experimental design set up.
4. The thermal conductivities attained for standard materials were consolidated on comparison with TPS measurements for standard materials. Then the methodology was applied to a 26650 Li-ion cell.
5. Results were compared with those published in [1]

Future Work:

1. Develop a two parameter model with lesser computation time.
2. Apply methodology to higher thermal conductivity materials.
3. Suggest appropriate cooling technique for a Li ion cell.

References

[1] Drake, S., Wetz, D., Jain, A., 'Measurement of anisotropic thermophysical properties of cylindrical Li-ion cells,' *Journal of Power Sources*, 252, 2014, pp. 298e304.

[2] Jason ,O., Shah, K., Jain, A., 'Measurement Sensitivity Analysis of the Transient Hot Source Technique Applied to Flat and Cylindrical Samples,' Journal of Thermal Science And Engineering Applications. 2017, Vol. 9 / 011002-5

[3] Z. Rao, S. Wang, 'A review of power battery thermal energy management,' Rev. 15 2011, 4554e4571.

[4] A.A. Pesaran, 'Battery thermal models for hybrid vehicle simulations,' J. Power Sources 110 (2002) 377e382.

[5]K. Smith, G.-H. Kim, E. Darcy, A. Pesaran, 'A Multi-Node Thermal System Model for Lithium-Ion Battery Packs,' Int. J. Energy Res. 34 (2010) 204e215.

[6] C. Forgez, D.V. Do, G. Friedrich, M. Morcrette, C. Delacourt, 'Thermal Modeling of Cylindrical LiFePO4 Batteries ,' J. Power Sources 195 (2010) 2961e2968.

[7] Y. Chen, J.W. Evans, 'Heat Transfer Phenomena in Lithium/Polymer-Electrolyte Batteries for Electric Vehicle Application,'J. Electrochem. Soc. 140 (1993)1833e1838.

[8] S.C. Chen, C.C. Wan, Y.Y. Wang, 'Thermal analysis of lithium-ion batteries,'J. Power Sources 140 (2005) 111e124.

[9] T.M. Bandhauer, S. Garimella, T. Fuller, 'A Critical Review of Thermal Issues in Lithium-Ion Batteries,' J. Electrochem. Soc. 158 (2011) R1eR25.

[10] (H. Maleki, S. A. Hallaj, J. R. Selman, R. B. Dinwiddie, and H. Wang, "Thermal properties of lithium-ion battery and components," J. Electrochem. Soc., vol. 146, no. 3, pp. 947–954, 1999.

Image References

[i] http://www.bbc.com/news/world-middle-east-11183476

[ii] https://www.cnet.com/news/why-are-hoverboards-exploding-and-catching-fire/

[iii] http://www.bbc.com/news/world-asia-39275826

[iv] http://www.telegraph.co.uk/news/aviation/10176808/Heathrow-Airport-closed-after-fire-breaks-out-on-Ethiopian-Airlines-Dreamliner-on-runway.html

[v] http://articles.latimes.com/2013/feb/07/business/la-fi-mo-boeing-787-dreamliner-ntsb-fire-20130207

[vi] Shah, Vishwakarma, et,al., JEECS 2016

[vii] Drake,et,a.,(2014)

[viii] http://batteryuniversity.com/learn/article/types_of_battery_cells

Biographical Information

Salwa Shaik, was born in Hyderabad, India. She received her Bachelors of Technology, in Mechanical Engineering, from the reputed Jawaharlal Nehru Technological University Anurag Group of Institutions, Telangana, India; in the year 2015. She then joined the University of Texas at Arlington during fall 2015, for her graduate studies in Mechanical Engineering. She started her research related to 'An improved method for measurement of radial thermal conductivity of cylindrical bodies' during the summer of 2016. Salwa received her Master of Science in Mechanical Engineering from the University of Texas at Arlington in May 2017.